Molecular Brightness Determined from a Generalized Form of Mandel's *Q*-Parameter

Alvaro Sanchez-Andres, Yan Chen, and Joachim D. Müller
School of Physics and Astronomy, University of Minnesota, Minneapolis, Minnesota 55455

ABSTRACT Mandel's *Q*-parameter, which is determined from the first two photon count moments, provides an alternative to PCH analysis for determining the brightness of fluorophores. Here, the definition of the *Q*-parameter is generalized to include correlations between photon counts that are separated by a time τ. We develop and experimentally verify a theory that takes the effects of dead time, afterpulsing, and the finite sampling time on the generalized parameter $Q(\tau)$ into account. $Q(0)$, which corresponds to the original *Q*-parameter, is severely affected by dead time and afterpulsing. $Q(\tau)$ for $\tau > 0$, on the other hand, is quite robust with respect to nonideal detector effects. Thus, analysis of $Q(\tau)$ provides a robust method for determining the brightness of fluorophores. We extend the theory to a mixture of species, which is characterized by an apparent brightness. The brightness of EGFP in CV-1 cells is measured as a function of protein concentration to demonstrate the feasibility of $Q(\tau)$ analysis in cells. In addition, we monitor protein association of the ligand-binding domain of retinoid X receptor in the presence and absence of 9-*cis*-retinoic acid by $Q(\tau)$ analysis.

INTRODUCTION

Fluorescence fluctuation spectroscopy (FFS) derives information about biomolecules from statistical analysis of fluorescence intensity fluctuations. A number of different FFS techniques exist and provide different information about the sample. Fluorescence correlation spectroscopy (FCS) is the most widely used technique and derives information about the dynamic properties of the sample from the correlation in the signal fluctuations (1,2). Other techniques, such as photon counting histogram (PCH) and cumulant analysis, target nondynamic properties of the sample (3,4). PCH analyzes the probability distribution function of the photon counts and determines the brightness of fluorescent molecules. The brightness of a fluorophore is given by the average number of photons emitted by one molecule over a specified time period. PCH analysis is useful for the study of particle aggregation and has been successfully applied to observe the oligomerization of proteins in living cells (5).

We briefly illustrate how brightness serves as a marker of the oligomeric state of a protein. A fluorescently labeled protein diffuses through the observation volume and produces a burst of detected photons. The average photon count rate of these bursts determines the molecular brightness of the labeled protein. If this protein associates to form a homodimer, the new complex will carry two fluorescent labels and produce on average twice as many photons as the monomeric protein. The molecular brightness of the dimer is therefore twice that of the monomer.

Protein oligomerization and aggregation are also measured by FCS, where changes in the diffusion coefficient induced by protein association are monitored by the autocorrelation function (for a review, see Thompson et al. (6)). Employing cross-correlation with dual-color detection provides a sensitive method for detecting protein interactions (7). Another approach uses the fluctuation amplitude $g(0)$ of the autocorrelation function to detect changes in the aggregation state of proteins (8,9). The idea behind this method is that the effective number of diffusing particles decreases upon oligomerization with respect to the monomer concentration. This results in an increase of the amplitude of the autocorrelation of the fluorescence intensity, which is used as a marker for oligomerization. More sophisticated setups and analysis methods, such as scanning FCS (8,10) and higher-order FCS (11,12), have been employed as well.

The degree of oligomerization depends on protein concentration. To monitor oligomerization by brightness, we measure the brightness over a wide concentration range. Because fluorescence intensity is proportional to concentration, we measure at intensities where dead-time effects of the detector become significant (13). This nonideal detector effect results in an artificial decrease in the brightness and leads to erroneous interpretation of PCH experiments. We developed an improved PCH theory that corrects for dead-time and afterpulsing effects and accurately determines brightness over a wide range of intensities (14).

An alternative to determining the brightness by PCH is moment analysis (11,15–17). Two approaches exist; the first directly calculates higher-order moments from the photon counts (17), whereas the other uses higher-order correlation functions to determine moments (11). Because moments and the probability distribution function used by PCH are mathematically equivalent, both methods provide the same information. Here we limit our discussion to the first two moments of the photon counts. They are sufficient to calculate the

Submitted May 20, 2005, and accepted for publication August 15, 2005.

Address reprint requests to Joachim Mueller, University of Minnesota, School of Physics and Astronomy, 116 Church St. SE, Minneapolis, MN 55455. Tel.: 612-625-4369; Fax: 612-624-4578; E-mail: mueller@physics.umn.edu.

0006-3495/05/11/3531/17 $2.00

doi: 10.1529/biophysj.105.067082

brightness of a single species. In the case of multiple species, the first two moments determine the apparent brightness of the sample, which represents an average brightness of all the species present in the solution (5). Moment analysis is attractive because it provides a very convenient and simple approach for computing the brightness. However, just as in the case of PCH, moment analysis suffers from dead time and afterpulsing of the detector. Equations that treat dead-time and afterpulsing effects on moment analysis have been introduced for the limit of short sampling times (14).

Moment analysis is based on Mandel's Q-parameter (18), which is defined in terms of the first two photon count moments. In this article we generalize Mandel's Q-parameter by including correlations between photon counts separated by a time τ. We develop the theory that connects the generalized Q-parameter $Q(\tau)$ to the brightness of fluorescent molecules for arbitrary sampling times and in the presence of detector dead time and afterpulsing. We also discuss the relationship between $Q(\tau)$ and the autocorrelation function. To test the theory we perform and analyze experiments using simple dye solutions.

The special case $Q(0)$ corresponds to the original definition of Mandel's Q-parameter. We extend the theory of Mandel's Q-parameter by including sampling time effects into the data analysis of $Q(0)$. Most importantly, we show that $Q(\tau > 0)$ is in contrast to $Q(0)$ remarkably robust against nonideal detector effects and only requires minor corrections to account for dead time and afterpulsing. Thus, the generalized Q-parameter provides an attractive method for analyzing brightness and is in several aspects superior to traditional analysis of the Q-parameter. We extend the theory of $Q(\tau)$ to include multiple species and introduce an approximation that provides a quick and convenient correction for dead-time effects. The low brightness and large protein concentrations typically encountered in cellular measurements present a challenge for PCH and conventional moment analysis (5). $Q(\tau)$ analysis, on the other hand, provides a robust method for determining the brightness of fluorophores in cells. We demonstrate the feasibility of $Q(\tau)$ analysis of cell data by determining the brightness of EGFP and by monitoring the protein association of a nuclear receptor.

THEORY

Mandel's parameter and brightness

PCH analysis provides a framework for determining the brightness ε in the limit of short sampling times. The brightness characterizes the number of photons received per molecule for a sampling time T. It is proportional to

$$\varepsilon = \lambda T, \tag{1}$$

in the short sampling time limit, where λ is the photon count rate of a single molecule (3). We previously treated both ε and λ as equivalent measures that determine the brightness of a molecule. However, ε depends explicitly on the sampling time and the simple relationship between ε and λ of Eq. 1 is not valid for long sampling times. The parameter λ, on the other hand, characterizes the instantaneous brightness of a molecule, which is independent of the sampling time. Thus, we focus on the brightness λ in this article.

Moment and cumulant analysis provide an alternative for determining the brightness (4,17). We assume in the following a single diffusing species with a photon count rate of λ. The brightness of a single species in the limit of short sampling times is readily determined from Mandel's Q-parameter (3,18)

$$Q = \frac{\langle k^2\rangle - \langle k\rangle^2 - \langle k\rangle}{\langle k\rangle} = \gamma_2\varepsilon = \gamma_2\lambda T, \tag{2}$$

where γ_2 is a shape factor that depends on the point spread function $PSF(\vec{r})$ (8). The factors γ_r are defined by

$$\gamma_r = \frac{\int \mathrm{PSF}^r(\vec{r})d\vec{r}}{\int \mathrm{PSF}(\vec{r})d\vec{r}}. \tag{3}$$

If the PSF is normalized, $PSF(0) = 1$, its volume $V_{\mathrm{PSF}} = \int PSF(\vec{r})dr^3$ corresponds to the observation volume typically employed in FCS experiments, and the brightness λ and the average number of fluorophores N in the observation volume is proportional to the average of the photon counts, $\langle k\rangle = \lambda NT$ (3).

Although calculation of the brightness from the photon count moments of Eq. 2 is fast and convenient, previous work has shown that this method suffers from dead-time and afterpulsing effects of the photodetectors and yields inaccurate values of the brightness even at relatively low concentrations (14). An algorithm based on a first-order Taylor expansion that takes nonideal detector effects for short sampling times into account has been described (14).

Generalized Mandel's parameter $Q(\tau)$

We now introduce an alternative method for calculating the brightness λ. It utilizes the photon count correlation function,

$$g_k(\tau) = \frac{\langle k(t)k(t+\tau)\rangle - \langle k\rangle^2 - \langle k\rangle\delta_{0,\tau}}{\langle k\rangle^2}, \tag{4}$$

where $\delta_{0,\tau} = 0$ for $\tau \neq 0$ and $\delta_{0,\tau} = 1$ for $\tau = 0$. The function $\delta_{0,\tau}$ was introduced to subtract the shot noise term for $\tau = 0$. The symbol $k(t)$ is the number of photon counts registered in the sampling time interval $[t, t+T]$, and $\langle\ \rangle$ indicates averaging. The correlation between detected photons that are separated by a time of τ is given by $\langle k(t)k(t+\tau)\rangle$. The photon count correlation function $g_k(\tau)$ is identical to the fluorescence intensity correlation function $g_I(\tau)$ of FCS in the short sampling time limit. We now introduce a generalization of Mandel's Q-parameter by multiplying $g_k(\tau)$ with $\langle k\rangle$,

$$Q(\tau) = g_k(\tau)\langle k\rangle = \frac{\langle k(t)k(t+\tau)\rangle - \langle k\rangle^2 - \langle k\rangle\delta_{0,\tau}}{\langle k\rangle}. \tag{5}$$

We develop in the following expressions that relate $Q(\tau)$ to the brightness λ. In addition, we consider the effect of sampling time T, detector dead time $\tau_\dagger$, and afterpulsing on $Q(\tau)$. We will see in the following that $Q(0)$ and $Q(\tau>0)$ behave very differently, and it becomes necessary to treat each case separately. We use Q_0 to refer to $Q(\tau=0)$ and Q_τ to refer to $Q(\tau>0)$. Note that Q_0 is equal to the traditional Q-parameter.

The statistics of the photoelectron counts is closely related to the statistics of the integrated intensity

$$W(t)=\int_{-T/2}^{+T/2} I(t+t^*)dt^*. \tag{6}$$

If the intensity $I(t)$ does not vary significantly over the sampling time period T, Eq. 6 simplifies to

$$W(t)=I(t)T. \tag{7}$$

The validity of Eq. 7 specifies the short sampling time limit. In other words, the short sampling time limit requires that the timescale of intensity fluctuations is much larger than the sampling time. For purely diffusing fluorophores, the characteristic timescale of fluctuations is given by the diffusion time τ_D. Thus, the short sampling time limit is valid for sampling times that are much shorter than the diffusion time $T \ll \tau_D$. In this limit the photon count correlation function equals the fluorescence intensity correlation function,

$$g_k(\tau)=g_I(\tau)=\frac{\langle I(t)I(t+\tau)\rangle-\langle I\rangle^2}{\langle I\rangle^2}. \tag{8}$$

However, in the following we will mainly consider long sampling times where Eq. 8 is no longer valid. We later discuss the relationship between $g_I(\tau)$ and the generalized Mandel's parameter $Q(\tau)$.

In the absence of dead time, the probability distribution function (pdf) of the integrated intensity $p(W)$ is related to the pdf of the photon counts $p(k)$ by Mandel's formula (19)

$$p(k)=\int p(W)Poi(k,W)dW, \tag{9}$$

where $Poi(k,x)$ is the Poisson distribution with average x.

Notation

To be consistent with previous work (14), we label dead-time-affected variables with a prime and afterpulsing affected variables with a star. For example, we denote the ideal pdf of observing k photons during the sampling time T by $p(k)$, whereas the afterpulsing and dead-time-affected pdf is referred to as $p'^*(k)$.

Dead-time effect on the generalized *Q*-parameter

Dead-time influences the moments of the photon counts and therefore changes the Q-function

$$Q'(\tau)=\frac{\langle k_0k_\tau\rangle'-\langle k\rangle'^2-\langle k\rangle'\delta_{0,\tau}}{\langle k\rangle'}. \tag{10}$$

Equation 10 has the same form as Eq. 5, but every moment is replaced by the dead-time-affected moment. In addition, we introduced a shorthand notation, where $k(t)$ is written as k_t. We also assumed a stationary process, so that correlations only depend on the time difference τ. Dead time does not change the fact that photon detection is a doubly stochastic process, and the probability distribution functions of k and W are related by

$$p'(k)=\int p(W)P'(k|W)dW, \tag{11}$$

which generalized to a bivariate distribution function is given by

$$p'(k_0,k_\tau)=\int\int p(W_0,W_\tau)P'(k_0|W_0;k_\tau|W_\tau)dW_0dW_\tau. \tag{12}$$

In the absence of dead time the detection process of each photon is statistically independent from the detection process of others, which yields a Poissonian probability function $P(k|W)=Poi(k,W)$ (19). However, dead-time effects destroy the statistical independence of the detection process. After the detection of one photon event, no other can be detected for a period of time equal to the dead time. As a result, the dead-time-affected conditional probability $P'(k|W)$ is no longer Poissonian.

O'Donell (20) developed an analytical expression for $P'(k|W)$ using a Taylor expansion in the dead-time parameter δ for nonparalyzable detectors. The parameter δ is defined as the quotient of the dead time $\tau_\dagger$ and the sampling time ($\delta=\tau_\dagger/T$). The expression to first order in δ is

$$P'(k|W)\simeq Poi(k,W)\{1+\delta[kW-k(k-1)]\}. \tag{13}$$

The bivariate conditional probability $p'(k_0|W_0;k_\tau|W_\tau)$ of detecting k_0 photons given an integrated intensity of W_0 and of detecting k_τ photons a time τ later given an integrated intensity of W_τ is given by

$$P'(k_0|W_0;k_\tau|W_\tau)\simeq P'(k_0|W_0)\times P'(k_\tau|W_\tau). \tag{14}$$

The detection of photons is essentially instantaneous, but dead time introduces a statistical dependence for times less than the dead time. Thus, as long as $\tau>\tau_\dagger$ and for integrated intensities W_0 and W_τ that do not temporally overlap ($\tau\geq T$) Eq. 14 is valid. These conditions are always fulfilled in our experiments.

A consequence of Mandel's formula is that the factorial moments of the photon counts are identical to the moments of the integrated intensity (21), $\langle k(k-1)\dots(k-r)\rangle=\langle W^{r+1}\rangle$. If we use this relationship and combine Eqs. 13 and 14 with Eqs. 11 and 12, we obtain a relation between the dead-time-affected moments of the photon counts and the ideal moments of W,

$$\langle k_0 k_\tau\rangle' = \sum_{k_0,k_\tau} k_0 k_\tau p'(k_0,k_\tau) = \langle W_0 W_\tau\rangle - 2\delta\langle W_0^2 W_\tau\rangle$$
$$\langle k\rangle' = \sum_{k} k\, p'(k) = \langle W\rangle - \delta\langle W^2\rangle, \quad (15)$$

where we used $\langle W_0^2 W_\tau\rangle = \langle W_0 W_\tau^2\rangle$. Next, we express the ordinary moments of W as cumulants of W (see Appendix A), where $\langle\langle\ \rangle\rangle$ denotes the cumulant. Thus, Eq. 15 written in terms of integrated intensity cumulants is

$$\langle k_0 k_\tau\rangle' - \langle k_0\rangle'^2 = \langle\langle W_0 W_\tau\rangle\rangle - 2\delta(\langle\langle W_0^2 W_\tau\rangle\rangle + 2\langle\langle W\rangle\rangle\langle\langle W_0 W_\tau\rangle\rangle)$$
$$\langle k\rangle' = \langle\langle W\rangle\rangle - \delta(\langle\langle W^2\rangle\rangle + \langle\langle W\rangle\rangle^2). \quad (16)$$

Inserting Eq. 16 into Eq. 10 and ignoring higher order terms in δ we arrive at an expression of the dead-time-affected Q-parameter for $\tau > 0$,

$$Q'_\tau(\tau) = \frac{\langle\langle W_0 W_\tau\rangle\rangle}{\langle\langle W\rangle\rangle} - \delta\left(3\langle\langle W_0 W_\tau\rangle\rangle + 2\frac{\langle\langle W_0^2 W_\tau\rangle\rangle}{\langle\langle W\rangle\rangle} - \frac{\langle\langle W_0 W_\tau\rangle\rangle\langle\langle W^2\rangle\rangle}{\langle\langle W\rangle\rangle^2}\right). \quad (17)$$

The introduction of cumulants in Eq. 17 is useful, because the integrated intensity cumulants are connected to properties of the sample,

$$\langle\langle W(t_1)W(t_2)\dots W(t_r)\rangle\rangle = \gamma_r(\lambda T)^r N f_T^{(r)}(t_1,t_2,\cdots,t_r), \quad (18)$$

as derived in Appendix A. We introduced in Eq. 18 the normalized correlation function of the integrated intensity

$$f_T^{(r)}(t_1,t_2,\cdots,t_r) \equiv T^{-r}\int_{t_1}^{T+t_1}\int_{t_2}^{T+t_2}\cdots\int_{t_r}^{T+t_r} f^{(r)}(t'_1,t'_2,\cdots,t'_r)dt'_1dt'_2\cdots dt'_r. \quad (19)$$

The function $f^{(r)}(t_1,t_2,\cdots,t_r)$ is closely related to the r-th order cumulant correlation function of the intensity,

$$\langle\langle I(t_1)I(t_2)\dots I(t_r)\rangle\rangle = \gamma_r(\lambda T)^r N f^{(r)}(t_1,t_2,\cdots,t_r). \quad (20)$$

Note, that $f^{(r)}(t_1,t_2,\cdots,t_r)$ is normalized ($f^{(r)}(0,0,\cdots,0) = 1$), because $\langle\langle I^r\rangle\rangle = \gamma_r(\lambda T)^r N$ (4). This implies according to Eq. 19 that $f_T^{(r)}(0,0,\cdots,0) \approx 1$ for short sampling times. The correlation function $f^{(r)}(t_1,t_2,\cdots,t_r)$ depends only on the shape of the point spread function and the physical process responsible for generating correlations. We assume throughout this article that the physical process is stationary, so that the correlation function depends on time differences only, $\tau_2 = t_2 - t_1, \tau_3 = t_3 - t_2, \cdots, \tau_r = t_r - t_{r-1}$. We now use the stationary property to rewrite the integrated intensity cumulant of Eq. 18

$$\langle\langle W(t_1)W(t_2)\dots W(t_r)\rangle\rangle = \gamma_r(\lambda T)^r N f_T^{(r)}(\tau_2,\tau_3,\cdots,\tau_r). \quad (21)$$

Inserting Eq. 21 into Eq. 17 allows us to finally arrive at an expression for the dead-time-affected Q-function for $\tau > 0$

$$Q'_\tau(\tau) = \gamma_2(\lambda T) f_T^{(2)}(\tau)\left(1 - \delta(\lambda T)\left(3N + 2\frac{\gamma_3}{\gamma_2}\frac{f_T^{(3)}(0,\tau)}{f_T^{(2)}(\tau)} - \gamma_2 f_T^{(2)}(0)\right)\right). \quad (22)$$

This equation is used to connect the experimentally determined Q'_τ with the brightness λ. In the absence of dead time ($\delta = 0$) Eq. 22 describes the ideal Q_τ parameter

$$Q_\tau(\tau) = \gamma_2(\lambda T) f_T^{(2)}(\tau). \quad (23)$$

The function $f_T^{(2)}(\tau)$ describes the sampling time dependence of the Q-parameter. The value of the function $f_T^{(2)}(T)$ tends to one in the limit of short sampling times. Thus, $Q_\tau(T) = \gamma_2\lambda T$ is identical to the original Q-parameter Q_0 (Eq. 2) in the limit of short sampling times.

To derive an expression for Q at $\tau = 0$, we start with Eq. 10 and repeat all of the above steps in the derivation of Q_τ, but evaluate the expressions for $\tau = 0$. Because of the shot noise term in $Q(0)$, and the unique dead-time dependence of each moment, we arrive at a very different expression to describe Q'_0. As we later show, Q'_0 is significantly more sensitive to dead-time effects than Q'_τ. We found that we need to include second-order terms in δ to describe experimental data accurately by Q'_0, whereas a first-order correction in δ is sufficient for Q'_τ. We describe in Appendix B the derivation of an expression for Q'_0 to second order in δ. The result is given by

$$Q'(0) = \lambda T(q_0 + q_1\delta + q_2\delta^2), \quad (24)$$

with

$$q_0 = f_T^{(2)}(0)$$
$$q_1 = 2N + \gamma_2 2 f_T^{(2)}(0) + \lambda T((\gamma_2 f_T^{(2)}(0))^2 - 3N\gamma_2 f_T^{(2)}(0) - 2\gamma_3 f_T^{(3)}(0,0))$$
$$q_2 = (N + \gamma_2 f_T^{(2)}(0)) + \frac{\lambda T}{2}(6N^2 + 25N\gamma_2 f_T^{(2)}(0) - 5(\gamma_2 f_T^{(2)}(0))^2 + 12\gamma_3 f_T^{(3)}(0,0)) + (\lambda T)^2\left(\gamma_2 f_T^{(2)}(0)(6N^2 + 3N\gamma_2 f_T^{(2)}(0) + (\gamma_2 f_T^{(2)}(0))^2) + f_T^{(3)}(0,0)(8N - 3\gamma_2 f_T^{(2)}(0)) + 3\gamma_4 f_T^{(4)}(0,0,0)\right). \quad (25)$$

In the limit of short sampling times, and by only keeping the first-order terms in δ, we recover the dead-time correction of moment analysis as previously described (14). Equations 24 and 25 extend the previous theory to second order and include the effects of sampling time on Q.

To calculate $Q(\tau)$ we need a physical model that describes our fluctuation experiments. We consider the case of diffusing molecules and assume a three-dimensional Gaussian (3DG) PSF. The second to fourth order normalized intensity correlation functions $f^{(\mathrm{r})}(\tau_2,\cdots,\tau_\mathrm{r})$ are given by Qian (16),

$$f^{(2)}_{3\mathrm{DG}}(\tau_2)=\left(1+\frac{\tau_2}{\tau_\mathrm{D}}\right)^{-1}\left(1+\frac{\tau_2}{r\tau_\mathrm{D}}\right)^{-1/2}\quad f^{(3)}_{3\mathrm{DG}}(\tau_2,\tau_3)=3\sqrt{3}\left(4\frac{\tau_2\tau_3}{\tau_\mathrm{D}^2}+4\frac{\tau_2+\tau_3}{\tau_\mathrm{D}}+3\right)^{-1}\left(4\frac{\tau_2\tau_3}{r^2\tau_\mathrm{D}^2}+4\frac{\tau_2+\tau_3}{r\tau_\mathrm{D}}+3\right)^{-1/2}$$

$$f^{(4)}_{3\mathrm{DG}}(\tau_2,\tau_3,\tau_4)=2\sqrt{2}\left(4\frac{\tau_2\tau_3\tau_4}{\tau_\mathrm{D}^3}+4\frac{\tau_2\tau_3+\tau_3\tau_4+\tau_2\tau_4}{\tau_\mathrm{D}^2}+\frac{3\tau_2+4\tau_3+3\tau_4}{\tau_\mathrm{D}}+2\right)^{-1}$$
$$\times\left(4\frac{\tau_2\tau_3\tau_4}{r^3\tau_\mathrm{D}^3}+4\frac{\tau_2\tau_3+\tau_3\tau_4+\tau_2\tau_4}{r^2\tau_\mathrm{D}^2}+\frac{3\tau_2+4\tau_3+3\tau_4}{r\tau_\mathrm{D}}+2\right)^{-1/2},\qquad(26)$$

where τ_D is the average diffusion time through the observation volume and r is the squared ratio of the radial and axial beam waist. The correlation functions $f^{(\mathrm{r})}_{2\mathrm{DG}}$ for a two-dimensional Gaussian (2DG) PSF are formally obtained from $f^{(\mathrm{r})}_{3\mathrm{DG}}$ by taking $r\to\infty$.

To calculate the dead-time-affected Q-function Q'_τ we need to evaluate $f^{(2)}_\mathrm{T}(\tau)$, $f^{(2)}_\mathrm{T}(0)$, and $f^{(3)}_\mathrm{T}(0,\tau)$ according to Eq. 22. To calculate Q'_0 requires the evaluation of $f^{(2)}_\mathrm{T}(0)$, $f^{(3)}_\mathrm{T}(0,0)$, and $f^{(4)}_\mathrm{T}(0,0,0)$. In general this requires numerical integration, however, it is possible to derive analytical solutions for special cases. We first consider the function $f^{(2)}_\mathrm{T}(\tau)$ and transform the integral of Eq. 19 using the fact that the integrand is stationary (4,22)

$$f^{(2)}_\mathrm{T}(\tau)=\frac{1}{T^2}\int_{-\mathrm{T}}^{+\mathrm{T}}(T-|t|)f^{(2)}(\tau+t)dt.\qquad(27)$$

For diffusing particles with a two-dimensional Gaussian PSF an analytical solution of $f^{(2)}_\mathrm{T}(\tau)$ is easily derived,

$$f^{(2)}_{2\mathrm{DG,T}}(\tau=0;x)=2x^{-2}\{x-(x+1)\mathrm{Log}(1+x)\}$$
$$f^{(2)}_{2\mathrm{DG,T}}(\tau>0;x)=\frac{(1+\tilde\tau)}{x^2}\mathrm{Log}\left[1-\frac{x^2}{(1+\tilde\tau)^2}\right]+\frac{1}{x}\left(\mathrm{Log}\left[\frac{\tilde\tau+x+1}{\tilde\tau-x+1}\right]\right),\qquad(28)$$

where we introduced the sampling factor $x=T/\tau_\mathrm{D}$ and $\tilde\tau=\tau/\tau_\mathrm{D}$. The functions $f^{(3)}_\mathrm{T}$ and $f^{(4)}_\mathrm{T}$, which are needed for the evaluation of Q'_τ and Q'_0, are evaluated numerically. We later discuss an approximation for Q'_τ, which only depends on $f^{(2)}_\mathrm{T}$ and therefore avoids the need for numerical integration.

Multiple species

Eqs. 22 and 24 describe the effect of dead time on the Q-function for a single species. It is straightforward to expand the theory to multiple species, because cumulant functions are additive for statistically independent variables (23),

$$\langle\langle W_{t_1}W_{t_2}\ldots W_{t_r}\rangle\rangle=\sum_\mathrm{i}\langle\langle W_{t_1}W_{t_2}\ldots W_{t_r}\rangle\rangle_\mathrm{i}$$
$$=\sum_\mathrm{i}\gamma_\mathrm{r}(\lambda_\mathrm{i}T)^\mathrm{r}N_\mathrm{i}f^{(\mathrm{r})}_{\mathrm{T,i}}(t_1,t_2,\cdots,t_\mathrm{r}).\qquad(29)$$

The subscript i characterizes parameters of the i-th species. We now explicitly derive an expression for $Q'(\tau>0)$ for multiple species. Using Eqs. 17 and 29 we get

$$Q'(\tau)=Q(\tau)-\delta\left(3\sum_\mathrm{i}\langle\langle W_0W_\tau\rangle\rangle_\mathrm{i}+2\frac{\sum_\mathrm{i}\langle\langle W_0^2W_\tau\rangle\rangle_\mathrm{i}}{\sum_\mathrm{i}\langle\langle W\rangle\rangle_\mathrm{i}}-\frac{\sum_\mathrm{i}\langle\langle W_0W_\tau\rangle\rangle_\mathrm{i}\sum_\mathrm{i}\langle\langle W^2\rangle\rangle_\mathrm{i}}{\left(\sum_\mathrm{i}\langle\langle W\rangle\rangle_\mathrm{i}\right)^2}\right).\qquad(30)$$

Inserting Eq. 21 into above equation allows us to model Q'_τ for multiple species. However, it is not possible to determine individual brightnesses from the parameter Q'_τ. Only a single brightness, which we refer to as apparent brightness, can be inferred. The apparent brightness λ_app is not a physical brightness, but represents the best average brightness of the mixture, and is defined by Mandel's Q-parameter, $Q=\gamma_2\lambda_\mathrm{app}T$ (15). The apparent number of molecules is determined from the average photon counts $\langle k\rangle=\lambda_\mathrm{app}TN_\mathrm{app}$. We now extend the concept of apparent brightness to $Q(\tau)$ analysis.

The diffusion coefficient of the individual species within a mixture often differs less than a factor of two, and we approximate the individual normalized intensity correlation functions of second order $f^{(2)}_\mathrm{T,i}(\tau)$ by an averaged correlation function $f^{(2)}_\mathrm{T}(\tau)$. We define N_app and λ_app by

$$\langle\langle W_0W_\tau\rangle\rangle=\sum_\mathrm{i}\gamma_2N_\mathrm{i}(\lambda_\mathrm{i}T)^2f^{(2)}_\mathrm{T,i}(\tau)=\gamma_2N_\mathrm{app}(\lambda_\mathrm{app}T)^2f^{(2)}_T(\tau)$$
$$\langle\langle W\rangle\rangle=\sum_\mathrm{i}N_\mathrm{i}\lambda_\mathrm{i}T=N_\mathrm{app}\lambda_\mathrm{app}T.\qquad(31)$$

Note that the ideal $Q_\tau=\langle\langle W_0W_\tau\rangle\rangle/\langle\langle W\rangle\rangle$ equals $\gamma_2\lambda_\mathrm{app}Tf^{(2)}_\mathrm{T}(\tau)$, which is consistent with our earlier definition for short sampling times, $Q_\tau(T)=\gamma_2\lambda_\mathrm{app}T$, because for short sampling times $f^{(2)}_\mathrm{T}(T)\approx1$. With this definition, we write Eq. 30 in terms of the apparent brightness and apparent number of particles:

$$Q'(\tau) \approx \gamma_2(\lambda_{\mathrm{App}}T)f_{\mathrm{T}}^{(2)}(\tau) - \delta\left(3N_{\mathrm{App}}\gamma_2(\lambda_{\mathrm{App}}T)^2 f_{\mathrm{T}}^{(2)}(\tau) + 2\frac{\sum_{\mathrm{i}}\langle\langle W_0^2 W_\tau\rangle\rangle_{\mathrm{i}}}{N_{\mathrm{App}}\lambda_{\mathrm{App}}T} - \gamma_2^2(\lambda_{\mathrm{app}}T)^2 f_{\mathrm{T}}^{(2)}(\tau)f_{\mathrm{T}}^{(2)}(0)\right). \quad (32)$$

We now introduce an approximation to express $\sum_{\mathrm{i}}\langle\langle W_0^2 W_\tau\rangle\rangle_{\mathrm{i}}$ in terms of N_{app} and λ_{app}

$$\sum_{\mathrm{i}}\langle\langle W_0^2 W_\tau\rangle\rangle_{\mathrm{i}} \approx \gamma_3(\lambda_{\mathrm{App}}T)^3 N_{\mathrm{App}} f_{\mathrm{T}}^{(3)}(0,\tau). \quad (33)$$

We will later discuss the validity of this approximation. Equation 32 together with Eq. 33 allow us to write an expression for Q'_τ, which is identical to the single species case (see Eq. 22, if one replaces the brightness and the number of molecules by their apparent parameters.

Afterpulsing

In addition to dead time, afterpulsing is another experimental artifact of the detector that affects PCH and moment analysis. An afterpulse constitutes a spurious photoelectron event that is triggered by the detection of a real event in the photodetector. The generation of afterpulses and its statistics has been studied in detail elsewhere (24,25). Its effects on PCH and moment analysis have also been characterized (14). The probability to observe an afterpulse at time t after a real event is characterized by a function $\alpha(t)$. The probability of observing an afterpulse decreases rapidly with increasing time t. Thus, $\alpha(t) \approx 0$ for t greater than a characteristic time t_0. For avalanche photodiode (APD) detectors, as commonly used in FFS experiments, the probability essentially drops to zero for times greater than a few microseconds. Hence, if we use a sampling time that is larger than the characteristic time t_0, we may safely assume that all afterpulses detected during a sampling period are caused by the real events detected in the same sampling period. In other words, there is no cross talk between neighboring sampling periods in terms of afterpulsing. We calculated in Appendix C the effect of afterpulsing on the generalized Mandel's parameter for sampling times larger than t_0. The effect of afterpulsing on the Q-function is given by

$$Q^*(\tau) = (1 + P_{\mathrm{a}})Q(\tau), \quad (34)$$

where P_{a} is the integrated probability of $\alpha(t)$ over the sampling period ($T > t_0$)

$$P_{\mathrm{a}} = \int_0^{\mathrm{T}} \alpha(t)dt \approx \int_0^{\infty} \alpha(t)dt. \quad (35)$$

MATERIALS AND METHODS

Instrumentation

A mode-locked Ti:sapphire laser (Tsunami, Spectra Physics, Mountain View, CA) pumped by an intracavity doubled Nd:YVO_4 laser (Spectra Physics) serves as source for two-photon excitation. The laser produces 100-fs pulses with a repetition frequency of 80 MHz (tunable between 700 and 1000 nm). The experiments were carried out using a Zeiss Axiovert 200 microscope (Thornwood, NY) with a 63× plan apochromat oil immersion objective (N.A. = 1.4). An excitation wavelength of 780 nm was used for the dye experiments, and a wavelength of 905 nm was used for the cell measurements. The power at the sample was determined by measuring the laser power directly after the objective. The excitation power was <3 mW for solution measurements, and was 0.25 mW for cell measurements. No photobleaching was detected for any of the samples measured. A dichroic filter (Chroma Technology, Brattleboro, VT) was used to separate the fluorescence from the excitation light. Photon counts were detected with an avalanche photodiode (SPCM-AQ-14, PerkinElmer, Vaudreuil, Quebec). The output of the APD, which produces TTL pulses, was directed to a data acquisition card (ISS, Champaign, IL). The card records the complete sequence of photoelectron counts to computer memory. The data shown were taken using sampling times between 10 and 200 μs. The data were analyzed using programs written for IDL version 5.4 (Research Systems, Boulder CA).

Sample preparation

Alexa488 was purchased from Molecular Probes (Eugene, OR) and dissolved in pure water. Initial concentrations of the stock solutions were determined from absorption measurements using the excitation coefficients provided by Molecular Probes. Samples for the FFS experiments were prepared by diluting the stock solution either in water or in a 60:40 (v/v) glycerol/water solution.

CV-1 cells were obtained from ATCC (Manassas, VA) and maintained in 10% fetal bovine serum (Hyclone Laboratories, Logan, UT) and EMEM media. EGFP-C1 and EGFP-RXRLBDβ vectors were generated as described previously (5). Transfections were carried out by using transfectin (Bio-Rad, Hercules, CA) according to manufacturer's instructions. Cells were subcultured into eight-well coverglass chamber slides (Naglenunc International, Rochester, NY) 48 h before measurements. Before measurements, the growth media was exchanged to Leibovitz's L-15 medium (no phenol red) with 10% fetal bovine serum (Invitrogen, Carlsbad, CA); 9-*cis* retinoic acid (Sigma-Aldrich, St. Louis, MO) was added to the media at 300 nM concentration. FFS measurements were performed 5 min after the addition of ligand.

Data analysis

Q'_0 is directly determined from the photon count moments of the FFS data. The generalized Q-function $Q'(\tau)$ is calculated from the raw data according to Eq. 10 for $\tau = T$. The dead time of the detector was determined by exposing it to light of ~10 kcps and observing the output signal with a digital oscilloscope (Tektronix TDS 3034, Wilsonville, OR). The dead time is determined by the shortest time interval between consecutive pulses. We found a value of 50 ± 1 ns, which agrees with the manufacturer's specification. The autocorrelation function of the FFS data was used to determine the diffusion time of the fluorophores.

Our goal is to determine the brightness λ from the experimentally measured dead-time-affected Q-value. However, the mathematical models for Q'_0 and Q'_τ depend on both the brightness and the number of molecules, $Q'(\lambda, N)$. Thus, to determine the brightness we need another experimental observable. This observable is the dead-time-affected average number of photon counts $\langle k\rangle'$. According to Eq. 15 $\langle k\rangle'$ is given by

$$\langle k\rangle' = \lambda TN(1 - \delta\lambda T(\gamma_2 f_{\mathrm{T}}^{(2)}(0) + N)). \quad (36)$$

We solve above equation for N,

$$N = \frac{1}{2\delta\lambda T}\Big\{(1 - \gamma_2\delta\lambda T f_T^{(2)}(0)) - \sqrt{(1 - \gamma_2\delta\lambda T f_T^{(2)}(0))^2 - 4\delta T\langle k\rangle'}\Big\}. \quad (37)$$

Inserting Eq. 37 into the formulas for $Q'(\lambda, N)$, we find an equation that only depends on the brightness and is solved numerically. The algorithms for data analysis were implemented into programs written in IDL language and used for data and error analysis. Errors in both Q'_0 and Q'_τ were determined experimentally by dividing each data set into segments of equal length, and the value of the Q-parameter was calculated for each segment. We determined the standard deviation and mean of the Q-parameters for data analysis.

The functions $f_T^{(r)}$ depend on the diffusion time τ_D, which is determined from analysis of the autocorrelation function. We empirically found that the diffusion time is a robust parameter that is little affected by dead-time effects. The determination of the diffusion time from experimental data is reliable as long as we make sure that photobleaching is absent. We calibrated the observation volume V_{PSF} by measuring an Alexa488 solution of known concentration c and determined N and λ from Q'_τ and $\langle k\rangle'$ according to Eqs. 22 and 37. The volume is determined by $N = cV_{PSF}$.

RESULTS AND DISCUSSION

Dead-time effects on Q_τ and Q_0

Let us first compare traditional moment analysis, which uses the Q_0 parameter, with Q_τ-correlation analysis. To simplify the comparison we neglect afterpulsing and undersampling, and concentrate on the effects of dead time only. In the absence of dead time we would measure the ideal $Q_\tau(\tau)$ value. Dead time leads to a biased value $Q'(\tau)$. The relative deviation $r_Q(\tau) \equiv (Q'(\tau) - Q(\tau))/Q(\tau)$ captures the bias introduced by deadtime. Let us evaluate $Q(\tau)$ for $\tau = T$ and $\tau = 0$. We refer to the generalized Q-parameter at $\tau = T$ as Q_T. Note that in the short sampling time limit $f_T^{(r)} = f^{(r)}$. In addition, $f^{(r)} \approx 1$ for correlation times $\tau \ll \tau_D$. Because the times $\tau = T$ and $\tau = 0$ are much less than τ_D, all functions $f_T^{(r)}$ in Eqs. 22 and 25 are set equal to one, which results in very simple equations. Fig. 1 shows the dead time induced relative deviation $r_Q(T)$ together with $r_Q(0)$ for traditional moment analysis as a function of fluorescence intensity $\langle I\rangle$. We calculated Q_T and Q_0 in the limit of short sampling times according to Eqs. 22 and 24 for a brightness of $\lambda = 10{,}000$ cps, a sampling time $T = 10\ \mu$s, and a dead time of 50 ns, which corresponds to a dead-time parameter δ of 0.005. These are values we typically encounter in actual experiments. The number of molecules N was varied, which translates into intensity as $\langle I\rangle = \lambda N$. Fig. 1 shows the behavior of r_Q up to intensities of 2×10^6 cps, which is close to the upper limit of most photon counting experiments. At low intensities the relative deviation is small for both, Q_T and Q_0, because dead-time effects are negligible in this regime. Both Q-values decrease with increasing intensity due to dead time, but the r_Q of Q_T is much less than that of Q_0. For example, an intensity of 300,000 cps leads to a dead-time-induced relative deviation of 100% for Q_0, whereas Q_T experiences only a relative decrease of 5% at the same intensity.

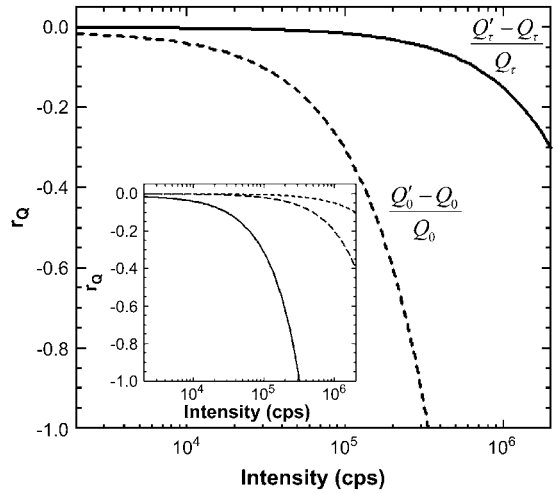

FIGURE 1 Relative deviation of Q_0 (*dashed line*) and Q_T (*solid line*) introduced by dead time as a function of fluorescence intensity in the short sampling time limit for $\lambda = 10$ kcsm, $T = 10\ \mu$s, and $\tau_\dagger = 50$ ns. The inset shows the relative deviation of the numerators of Q_0 (*solid line*) and Q_τ (*dashed line*), as well as of the common denominator $\langle k\rangle'$ (*dotted line*) as a function of the fluorescence intensity.

To better understand the difference in the behavior of Q'_0 and Q'_T for $\tau > 0$, we take a closer look at the moments used to calculate them. Both definitions differ in their numerator, $\langle \Delta k^2\rangle' - \langle k\rangle'$ for Q_0 and $\langle \Delta k(t)\Delta k(t+T)\rangle'$ for Q'_T. The relative deviation of both numerators due to dead time is shown as an inset of Fig. 1 as a function of intensity. The figure clearly demonstrates that the second factorial moment $\mu_{[1,1]}(\tau) = \langle \Delta k(t)\Delta k(t+\tau)\rangle$ is significantly less affected by dead time than the second factorial moment $\mu_{[2]} = \langle \Delta k^2\rangle - \langle k\rangle$. Thus the primary reason for the robustness of Q_T versus Q_0 analysis lies in the different transformation behavior of the factorial moments with respect to dead time. We also show the dead-time-induced relative deviation of the average number of photon counts $\langle k\rangle$ for comparison.

To experimentally mimic the situation where only dead time affects Q_τ, we prepared a dye solution in a glycerol/water mixture. FCS analysis of the sample determined a diffusion time of 425 μs (data not shown). We measured the dye solution using a sampling time of $T = 10\ \mu$s and determined Q'_T. This measurement was repeated after each dilution of the sample and the corresponding Q'_T is shown as a function of the fluorescence intensity in Fig. 2. The value of Q'_T decreases with increasing intensity as expected. Because the diffusion time is much larger than the sampling time, we are in the short sampling time limit. Note that the experimental fluorescence intensity is altered by dead time, $\langle I\rangle' = \langle k\rangle'/T$, albeit only slightly. We accounted for this bias while fitting the data to Eq. 22. The solid line is a description of the data by theory for a dead time of $\tau_\dagger = 50$ ns and a brightness of $\lambda = 18.36 \pm 0.04$ kcps. Our theory successfully describes the experimentally observed Q'_T.

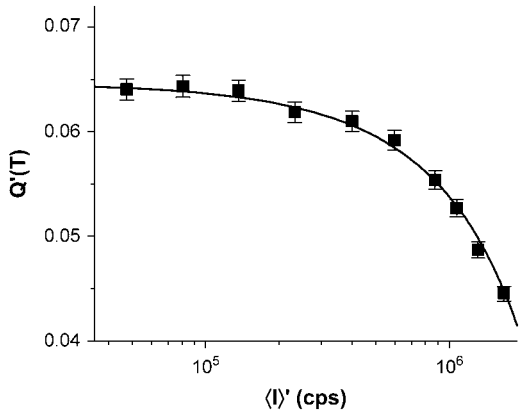

FIGURE 2 Dilution experiment of Alexa488 in a 60:40 (v/v) glycerol/water mixture. After each dilution the sample is measured with a sampling time of $T = 10\,\mu$s. The parameter Q'_T was evaluated for each measurement and is graphed as a function of the experimentally collected fluorescence intensity $\langle I\rangle'$. A diffusion time of 425 μs was determined by autocorrelation analysis. Because $T/\tau_D \ll 1$ we fit the data to Eq. 22 in the limit of short sampling times. The fit (*solid line*) with a reduced χ^2 of 1.1 determines a brightness of 18.36 ± 0.04 kcps.

Dead time and sampling time dependence of $Q(\tau)$

Most experiments are performed in aqueous solution, where the diffusion time is much faster than in glycerol mixtures. As a consequence the effect of sampling time on $Q(\tau)$ usually has to be accounted for. To test our theory in this regime we performed a dilution experiment on an aqueous Alexa488 solution with a sampling time of $T = 40\,\mu$s. The diffusion time of the sample is 40 μs as determined from the autocorrelation function, which results in a sampling factor $x = T/\tau_D = 1$. The value of $Q(T)$ as a function of intensity is shown in Fig. 3 *A* together with the best fit of the data to Eq. 22 for a dead time of 50 ns. The fit determined a brightness of $\lambda = 8.66 \pm 0.04$ kcps and describes the data within experimental error.

To demonstrate the robustness of our technique with respect to sampling time, we rebinned the received photon counts in software by adding together neighboring photon counts to get a new sequence with a twice longer sampling time. The sampling time of the new sequence is $T_R = 80\,\mu$s, which results in strong undersampling with a sampling factor $x = 2$. We graph in Fig. 3 *B* $Q(T_R)$ as a function of intensity. The solid line represents the best fit of the data to Eq. 22 with a dead time of 50 ns. Again, theory and experiment agree with one another. Because brightness is a property of the dye we expect it to be independent of the sampling frequency. The fitted brightness of $\lambda = 8.71 \pm 0.04$ kcps for a sampling time of 80 μs is in excellent agreement with the brightness determined for a sampling time of $T = 40\,\mu$s, and provides an additional check of the theory.

After we demonstrated that the theory describes the dead-time-affected Q-parameter, we now apply the theory to directly determine the brightness for each measurement. Fig. 3 *C* shows the brightness for each dilution measurement presented in Fig. 3, *A* and *B*, as a function of the fluorescence intensity. The brightness was determined from Q'_T and $\langle k\rangle'$

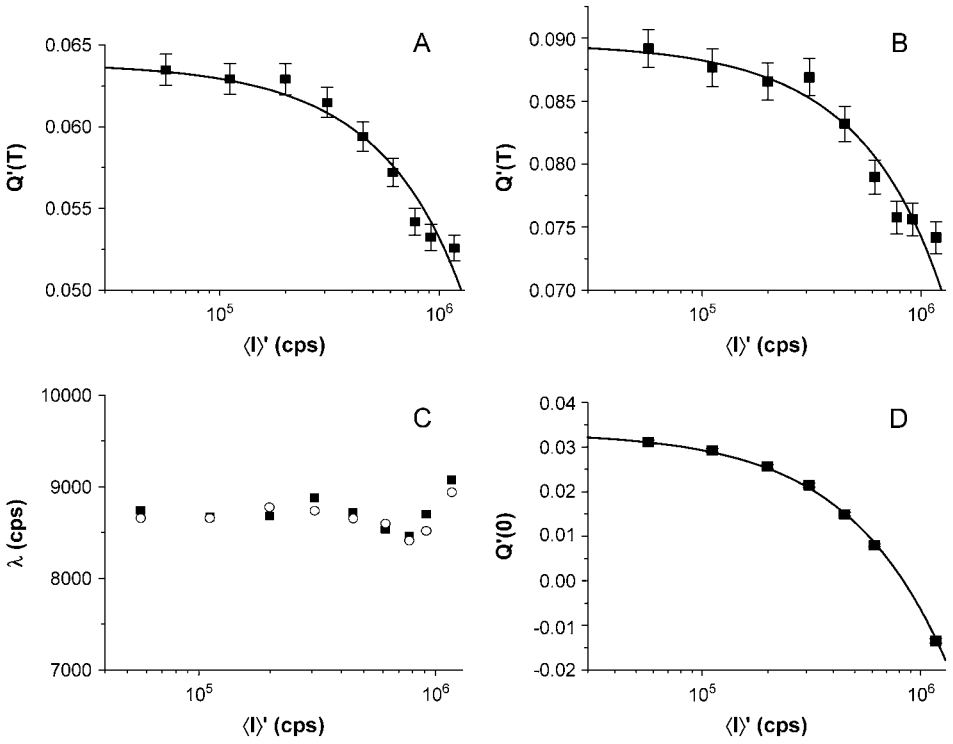

FIGURE 3 Dilution experiment of Alexa488 in water. The dye solution is measured with a sampling time of 40 μs and is repeatedly diluted in-between measurements. (*A*) The parameter Q'_T is graphed as a function of the fluorescence intensity $\langle I\rangle'$ and fit to Eq. 22 using a diffusion time of 40 μs as determined by autocorrelation analysis. The brightness determined by the fit (*solid line*) is 8.66 ± 0.04 kcps. (*B*) The fluctuation data are rebinned to a sampling time of 80 μs, and Q'_T is reanalyzed for the new sampling time. The fit (*solid line*) of the data to Eq. 22 yields a brightness of 8.71 ± 0.04 kcps. (*C*) The brightness of each individual measurement of Q'_T presented in panels *A* and *B* is directly calculated from Eq. 22. The circles and squares represent the brightness determined from Q'_T with sampling times of 40 μs and 80 μs, respectively. (*D*) Q'_0 is plotted as a function of the intensity $\langle I\rangle'$ for a sampling time of 40 μs. The data are fit to Eq. 24, using a dead time of $\tau_\dagger = 51$ns after correcting for afterpulsing with Eq. 72. The fit (*solid line*) with a reduced $\chi^2 = 1.2$ leads to a brightness of 8.84 ± 0.05 kcps.

as described in Materials and Methods and corrects for undersampling and dead time. The brightness of the dye is concentration independent as expected. Note that intensity is proportional to the dye concentration. The brightness recovered for the two different sampling times is within error identical and concentration independent, as expected.

Q(*T*) analysis versus *Q*(0) analysis

We reanalyze the Alexa488 dilution experiment in the glycerol-water mixture, but use Q_0 instead of Q_T analysis. Because we are in the short sampling time limit, all functions $f_T^{(r)}$ are set to one during the analysis. We determine the molecular brightness from the experimental value Q'_0 by solving Eq. 24 for λ. The brightness determined by Q_0 analysis is graphed in Fig. 4 together with the brightness earlier determined by Q_T analysis. We expect to recover the same brightness independent of the analysis technique employed, but observe a significantly higher brightness for Q_0 analysis than for Q_T. Both Q-values have been corrected for dead time. However, we neglected so far the effect of afterpulsing on the Q-parameter. If we apply the correction due to afterpulsing on Q_0 as described in Eq. 72 of Appendix C, we arrive at a brightness curve (*dashed line*) in Fig. 4, which is within error identical to the brightness determined by Q_T ($\lambda = 18.5 \pm 0.1$ kcps for Q_0 analysis and $\lambda = 18.36 \pm 0.04$ kcps for Q_T analysis).

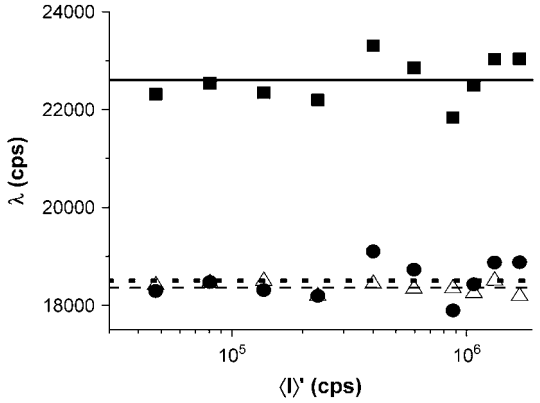

FIGURE 4 Brightness of Alexa488 in a 60:40 (v/v) glycerol/water mixture as a function of intensity $\langle I \rangle'$. Undersampling effects are negligible for this sample. The open triangles represent the brightness calculated by Q_T analysis from Eq. 22, whereas the squares correspond to the brightness calculated by Q_0 analysis from Eq. 24. The brightness calculated from Q_0 exceeds the brightness based on Q_T. Including afterpulsing effects in Q_0 analysis by Eq. 72 lowers the calculated brightness (●) to the values determined by Q_T analysis. The lines indicate the value of the average brightness of the dilution data for each analysis technique. The average brightness (*dashed line*) of Q_T analysis corrected for dead time yields 18.36 ± 0.04 kcps, whereas the average brightness (*dotted line*) based on Q_0 analysis corrected for dead time and afterpulsing is 18.5 ± 0.1 kcps. The average brightness (*solid line*) of Q_0 analysis without afterpulse correction is 22.6 kcps.

Note that so far we have not corrected Q_T for afterpulses. The fact that both brightness values match implies that the effect of afterpulsing on Q_T is very weak. In fact, Eq. 34 states that correcting Q_τ for afterpulses is equivalent with multiplying Q_τ with the factor $(1+P_a)$. The cumulative afterpulsing probability of the APD used for this experiment was determined to be 0.007. In other words, correcting Q_T for afterpulsing effects changes its value by $<1\%$, which is less than the experimental error. In other words, the effect of afterpulsing on Q_T can be safely ignored.

We assumed in our analysis that no undersampling is present and therefore $f_T^{(2)}(T) = 1$. A rigorous analysis that takes sampling time effects into account arrives at $f_T^{(2)}(T) = 0.98$ and $f_T^{(2)}(0) = 0.99$. The approximation of setting $f_T^{(2)}$ to one introduces a small error ($\sim 1\%$) in the brightness value. Note that by including undersampling in both Q_0 and Q_T the agreement of their brightnesses improves ($\lambda = 18.7 \pm 0.1$ kcps for Q_0 analysis and $\lambda = 18.76 \pm 0.04$ kcps for Q_T analysis).

We also performed Q_0 analysis on the Alexa488 measurements in aqueous solution, which we previously characterized by Q_τ analysis in Fig. 3 *A*. In contrast to Q_0 analysis in the glycerol/water mixture undersampling needs to be accounted for in this analysis. We fit the experimentally determined Q_0 values to Eq. 24 and accounted for afterpulsing using Eq. 72 (see Fig. 3 *D*). As we later discuss, Q_0 is very sensitive to the exact dead-time value of the photodetector. The best fit was obtained for a dead time of 51 ns, yielding a $\chi^2 = 1.2$ and a brightness of $\lambda = 8.8$ kcps, which is in good agreement with the value of 8.7 kcps obtained by Q_τ analysis.

Useful approximation for *Q*(*T*) analysis

Another complication of Q_0 analysis is the dependence of its dead-time-induced deviation on brightness. Lowering the brightness while keeping the intensity constant leads to an increase in the relative deviation. Fig. 5 shows the relative deviation r_Q of Q_0 for a brightness of 200 cps, 2000 cps, and 20,000 cps as a function of intensity. The deviation increases sharply with decreasing brightness. So far we have shown experimental data using Alexa488, which is a bright dye. However, many experimental conditions result in a lower brightness, such as the measurement of fluorescent proteins in cells. In this case, Q_0 analysis requires correction factors exceeding 100% even at moderate intensities. The slightest uncertainty in experimental parameters, such as the dead-time value, may introduce significant systematic errors.

In Fig. 5 we also plotted the relative deviation r_Q of Q_τ for a brightness of 200, 2000, and 20,000 cps as a function of intensity. All three curves overlap and are indistinguishable in the figure. Thus, the dead-time-induced relative deviation of Q_τ analysis is essentially independent of the brightness, whereas the dead-time-induced relative deviation of Q_0 is clearly brightness dependent.

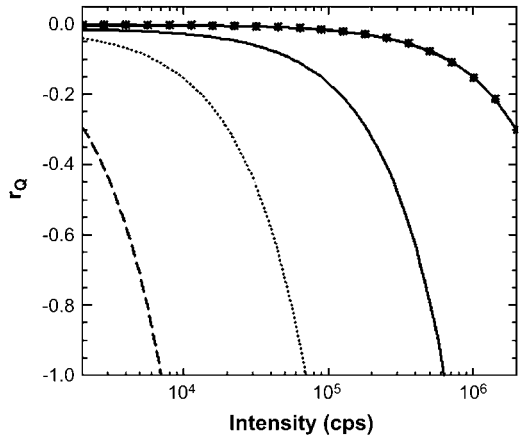

FIGURE 5 Relative deviation r_Q of Q_τ and Q_0 introduced by dead time for different brightness values as a function of intensity. The value of r_Q is calculated for a dead time of $\tau_\dagger = 50$ ns and for a sampling time of $T = 10$ μs in the absence of undersampling effects. The solid, dotted, and dashed lines represent r_Q of Q_0 for brightness values of 20,000, 2000, and 200 cps, respectively. The relative deviation of Q_τ for the same brightness values is plotted as symbols connected by lines. The relative deviation of Q_τ is virtually independent of the brightness, and all three curves overlap with each other.

This result suggests that, in practical terms, the intensity alone determines the relative deviation of Q_τ. To test this idea we use Eq. 22 and write r_Q as

$$r_{Q(\tau)} = \frac{Q'(\tau) - Q(\tau)}{Q(\tau)} = -(\phi_I + \phi_\tau), \tag{38}$$

with

$$\phi_I = 3N(\lambda T)\delta = 3\langle k\rangle\delta = 3\langle I\rangle\tau_\dagger$$
$$\phi_\tau = \delta(\lambda T)\left(2\frac{\gamma_3}{\gamma_2}\frac{f_T^{(3)}(0,\tau)}{f_T^{(2)}(\tau)} - \gamma_2 f_T^{(2)}(0)\right), \tag{39}$$

where we used $\langle I\rangle = \lambda N$ and $\tau_\dagger = \delta T$. The relative change of $Q(\tau)$ due to dead time is the sum of the two error functions ϕ_I and ϕ_τ. The function ϕ_I only depends on the intensity, whereas the second function ϕ_τ depends on the brightness λ and on the normalized integrated correlation functions. To better understand the magnitude of ϕ_τ, we first find an upper limit for ϕ_τ. The normalized integrated correlation function is always equal or less than one, $f_T^{(r)} \le 1$. In addition, higher order correlation functions decay faster than lower order ones. Thus, $f_T^{(3)}(0,\tau) \le f_T^{(2)}(\tau)$. This allows us to define the function $\bar{\phi}_\tau$,

$$\bar{\phi}_\tau \equiv \lambda\tau_\dagger\left(2\frac{\gamma_3}{\gamma_2}\right), \tag{40}$$

with $\bar{\phi}_\tau > \phi_\tau$. In other words, the function $\bar{\phi}_\tau$ overestimates the true contribution of ϕ_τ. We see that the value of $\bar{\phi}_\tau$ increases with the brightness λ. Using the γ-factors of a 3D Gaussian PSF and the deadtime of our detector ($\tau_\dagger = 50$ ns), a brightness of ~200 kcps is needed to get a relative deviation >1%. Such a high brightness is normally not encountered in FFS experiments. The brightness of all organic dyes we measured is <200 kcps. For instance, for in vitro experiments, the laser power must be kept low enough to avoid photobleaching, and we typically measure λ<100 kcps. For in vivo experiments on fluorescent proteins the brightness λ is usually <10 kcps. Moreover, intrinsic experimental errors are typically >1%, and it is safe to ignore the effect of ϕ_τ on the overall dead-time effect. Thus, we approximate the dead-time-induced relative deviation of $Q(\tau)$ as

$$r_{Q(\tau)} \approx -3N(\lambda T)\delta = -3\langle I\rangle\tau_\dagger. \tag{41}$$

A useful consequence of Eq. 41 is that the dead-time correction and the undersampling correction are independent from one another. In other words, it is possible to first correct for undersampling and then correct for dead-time effects. Thus, with this approximation we write Eq. 22 as

$$Q'(\tau) \approx \gamma_2\lambda T f_T^{(2)}(\tau)(1 - 3N\lambda T\delta). \tag{42}$$

We use Eq. 42 to analyze the experimental data. As discussed earlier, the approximation is valid for most FFS experiments. Only in the presence of extremely bright particles, such as quantum dots or complexes with a large number of fluorophores, is it necessary to check the validity of the approximation.

Multiple species

In the Theory section we extend Q_τ analysis from one species to multiple species. We demonstrated that the dead-time-affected Q'_τ for multiple species is described by the same expression valid for a single species, if the brightness and the number of molecules are replaced by their apparent parameters. To derive this expression we approximated $\sum_i \langle\langle W_0^2 W_n\rangle\rangle_i$ by Eq. 33. To investigate this approximation further, we consider the case of a binary mixture of two species with brightnesses λ_A and λ_B present at concentrations N_A and N_B. For these conditions the exact expression is

$$\sum_i \langle\langle W_0^2 W_n\rangle\rangle_i = \gamma_3 N_A \lambda_A^3 T^3 f_{T,A}^{(3)}(0,\tau) + \gamma_3 N_B \lambda_B^3 T^3 f_{T,B}^{(3)}(0,\tau). \tag{43}$$

The relative error e_r introduced by the approximation is thus given by

$$e_r = \frac{\sum_i \langle\langle W_0^2 W_n\rangle\rangle_i - \gamma_3 N_{app}\lambda_{app}^3 T^3 f_T^{(3)}(0,\tau)}{\sum_i \langle\langle W_0^2 W_n\rangle\rangle_i}$$
$$= \frac{f(f-1)(r-1)^2 r}{((r-1)f+1)((r^3-1)f+1)}, \tag{44}$$

where we introduced the fractional concentration $f = N_A/(N_A+N_B)$ and the brightness ratio $r = \lambda_A/\lambda_B$ of the two species.

The relative error introduced by the approximation only depends on the brightness ratio and the fractional concentration of both species. Because we are interested in applying Q_τ analysis in cells to probe the oligomerization of proteins, we investigate the relative error of a monomer-dimer and a monomer-tetramer mixture. The brightness ratio r of the monomer/dimer system is two and that of the monomer/tetramer system is four. In Fig. 6 we plot the relative error introduced by the approximation for the two systems. The worst case introduces an error of 35% for the monomer/tetramer sample, and an error of 11% for the monomer/dimer mixture. It is easy to show that the maximum of the relative error grows with increasing brightness ratio and reaches a limiting value of 100%.

With the approximation introduced in Eq. 33 we recover Eq. 22, if we substitute the molecular brightness and the number of molecules with their apparent parameters. As we discussed earlier for typical experimental conditions Eq. 22 is approximated by Eq. 42 with a relative deviation of $<1\%$. Note that Eq. 42 ignores the term $\sum\langle\langle W_0^2 W_n\rangle\rangle_i$. Thus, in the case of multiple species the relative error introduced by approximating $\sum\langle\langle W_0^2 W_n\rangle\rangle_i$ using an apparent brightness is usually less than a 35% bias of a term with a relative deviation of $<1\%$, and therefore unnoticeable given the experimental uncertainty of the data. Hence, the expression for Q'_τ in the presence of multiple species is well approximated by

$$Q'_\tau \approx \gamma_2(\lambda_{App}T) f_T^{(2)}(\tau)(1 - \delta 3 N_{App}(\lambda_{App}T)), \qquad (45)$$

which is identical to Eq. 42, if we substitute λ and N by their apparent values.

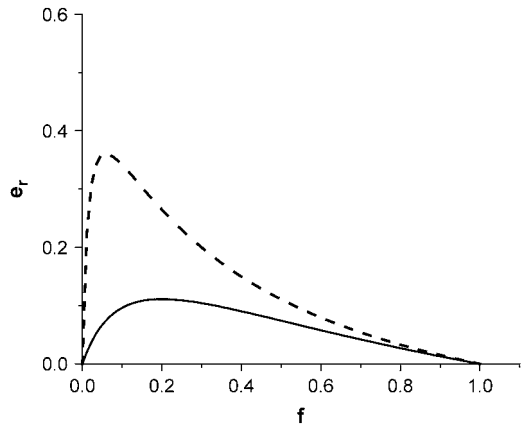

FIGURE 6 Relative error of $\sum\langle\langle W_0^2 W_\tau\rangle\rangle_i$ due to the approximation of Eq. 33 for a binary mixture. The introduction of an apparent brightness leads to a biased value of $\sum\langle\langle W_0^2 W_\tau\rangle\rangle_i$, which depends on the brightness ratio and the fractional concentration. The solid and dashed lines represent the relative error introduced by a monomer-tetramer and a monomer-dimer mixture as a function of the fractional concentration of the monomer. We used a brightness ratio of two for the dimer/monomer case and a ratio of four for the tetramer/monomer example.

Comparison of Q_τ and Q_0

Q_τ analysis of dead-time compromised data is much more stable than Q_0 analysis, because the correction factor required to recover the ideal parameter is much smaller for Q_τ than for Q_0. To illustrate the difference between both methods, we consider the effect of small uncertainties in dead time on the recovered brightness. We determined a dead time of $\tau_\dagger = 50$ ns for our detector with an uncertainty of ± 1 ns. Let us first generate dead-time-affected values of Q_τ and Q_0 for a dead time of exactly $\tau_\dagger = 50$ ns as a function of intensity. We chose a brightness of $\lambda = 1000$ cps and for simplicity ignore undersampling effects. Next, we use Eqs. 22 and 24 to determine the brightness from Q'_τ and Q'_0, but choose dead times of 49, 50, and 51 ns. This range of dead times is consistent with the experimental uncertainty. Fig. 7 shows the brightness recovered by Q_0 analysis as a function of intensity for the three different dead times. The brightnesses match at low intensities, where dead-time affects are less severe, but clearly start to deviate from one another with increasing intensity. The brightnesses determined for each dead time differ from one another by $>50\%$ for intensities over a million cps. Thus, Q_0 analysis is very sensitive to the exact value of the dead time. For comparison, we graph the brightnesses recovered by Q_τ analysis as a function of intensity for the three different dead times as an inset in Fig. 7. The difference between the brightness values is $<1\%$ even at an intensity of 2 million counts per second. This example

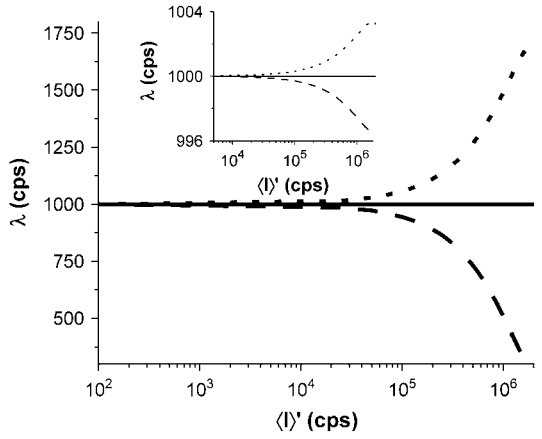

FIGURE 7 Robustness of Q_0 versus Q_τ analysis against uncertainties in the dead-time parameter. Q'_0 is calculated for a brightness $\lambda = 1000$ cps, a sampling time $T = 10\,\mu$s, and a dead time of $\tau_\dagger = 50$ ns as a function of N. Undersampling and afterpulsing effects are not considered here. We determine the brightness λ from Eq. 24 for three different dead times. The brightness recovered for dead times of 49 ns (*dashed line*), 50 ns (*solid line*), and 51 ns (*dotted line*) is shown as a function of the intensity $\langle I\rangle$, where $\langle I\rangle = \lambda N$. An uncertainty of ± 1 ns leads to an uncertainty of $>50\%$ in the brightness at high intensities. In contrast, repeating the calculation with the same parameters, but applying Q_τ analysis leads to an uncertainty of the brightness of $<1\%$. The inset shows the brightness determined by Q_τ analysis for dead times of 49 (*dashed line*), 50 (*solid line*), and 51 ns (*dotted line*).

shows that Q_τ is significantly more robust with respect to dead time than Q_0. In addition, as shown in Fig. 4 afterpulsing may severely affect Q_0, whereas its influence on Q_τ may be safely ignored in most cases. These advantages of Q_τ over Q_0 analysis lead us to abandon Q_0 analysis in favor of Q_τ.

In vivo applications of Q_τ analysis

We now demonstrate that brightness analysis by the Q_τ technique is feasible in living cells. We evaluate the generalized Q-parameter for $\tau = T$. CV-1 cells were transiently transfected with the fluorescent marker EGFP. Transfected cells are identified by using a conventional fluorescence microscope setup, which subsequently was switched to two-photon excitation for fluorescence fluctuation experiments. Data were collected with a sampling time of $T = 200\,\mu$s for a total of 30 s. The expression level of EGFP varies from cell to cell and is conveniently monitored by the fluorescence intensity, which is proportional to the protein concentration. By picking cells with different expression levels, it is possible to probe the concentration dependence of the molecular brightness. The dead-time-affected Q'_T and $\langle k \rangle'$ were calculated from the raw data of each measured cell. We used Eqs. 37 and 42 to determine the brightness λ and the number of molecules N of EGFP by correcting for undersampling and dead-time effects. The protein concentration was determined by $c = N/V_\mathrm{PSF}$ as discussed in Materials and Methods. The diffusion time of EGFP, which is needed for determining λ, was identified as $\tau_\mathrm{D} = 0.62$ ms from the autocorrelation function of the data. The brightness recovered from Q_T analysis of each measured cell is shown as a function of the protein concentration in Fig. 8 *A*. Our experiments cover EGFP concentrations from 200 nM to 5 μM. The molecular brightness of EGFP is constant throughout the measured concentration range as expected, because the photophysical properties of the fluorophore is independent of concentration. The average brightness of EGFP (*solid line* in Fig. 8 *A*) is 890 cps with a mean $\pm$ SD of 50 cps.

Next, we study the behavior of the ligand-binding domain RXRLBD of the nuclear receptor RXR. We performed measurements on CV-1 cells transfected with RXRLBD-EGFP, which is the ligand-binding domain tagged with the fluorescent protein EGFP. The first set of measurements was performed in the absence of the ligand 9-*cis*-retinoic acid. Data were taken and analyzed analogous to the EGFP measurements presented above. A diffusion time of 1.3 ms was measured for RXRLBD-EGFP in the absence of ligand. The dead time and undersampling corrected brightness of the receptor is graphed as a function of the EGFP concentration in Fig. 8 *B*. The apparent brightness of the protein is not constant, but increases as a function of protein concentration. The increase in the apparent molecular brightness indicates a change in the oligomeric composition of the protein solution. At low protein concentrations the molecular brightness

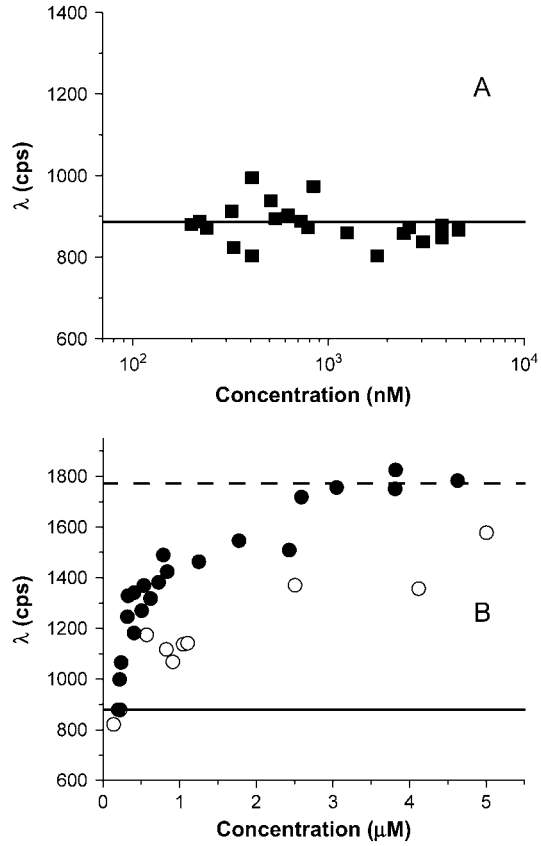

FIGURE 8 (*A*) Molecular brightness (■) of EGFP in CV-1 cells as a function of protein concentration. The brightness is determined by Q_T analysis from Eq. 42, where we accounted for dead-time and undersampling effects. Each data point represents the brightness measured in a different cell expressing EGFP. The concentration axis shows the total protein concentration expressed in terms of EGFP monomers. The brightness of EGFP is concentration independent with an average of ~890 cps (*solid line*) and a standard deviation of 50 cps. (*B*) Apparent brightness of RXRLBD-EGFP determined by Q_T analysis in the absence (○) and presence (●) of the ligand 9-*cis* retinoic acid. The concentration axis shows the total protein concentration expressed in terms of RXRLBD-EGFP monomers. The apparent brightness increases as a function of protein concentration in the absence of ligand. Addition of ligand leads to an increase in the apparent brightness and therefore promotes the formation of homodimers. The solid line indicates the brightness of monomeric EGFP, whereas the dashed line indicates the brightness of a homodimer.

of RXRLBD-EGFP is the same as the brightness of EGFP measured earlier (see Fig. 8 *A*). The match in brightness indicates that RXRLBD-EGFP proteins are not associating with one another. The increase of the apparent brightness with increasing protein concentration on the other hand requires the formation of homooligomeric protein complexes. If we assume a simple monomer/dimer equilibrium for RXRLBD-EGFP, the increase in the brightness is caused by an increase in the homodimer population of RXRLBD-EGFP. We expect for the limiting case of purely dimeric RXRLBD protein complexes an increase of the molecular brightness by a factor of two compared to the brightness of EGFP alone. We conclude that the protein has not reached

a purely dimeric composition in the experimentally accessible concentration range.

We added the ligand 9-*cis* retinoic acid, which activates the nuclear receptor RXR, to the cell culture to monitor changes in the oligomerization state of the receptor upon activation. Data were taken and analyzed as in the case without ligand. We obtained in the presence of ligand a diffusion time of 8 ms for RXRLBD-EGFP. The corrected apparent brightness is graphed as a function of EGFP concentration in Fig. 8 *B* as solid symbols. The apparent brightness of RXRLBD-EGFP at the lowest concentration corresponds to a monomeric protein. The apparent molecular brightness increases with protein concentration and reaches a limiting value that is twice the brightness of EGFP. This suggests that RXRLBD forms homodimers and that at high concentrations all RXRLBD proteins are homodimers. Note that the apparent brightness in the presence of ligand exceeds the brightness measured without ligand. In other words, the addition of ligand promotes the formation of RXRLBD homodimers.

The results of the in vivo study of RXRLBD in CV-1 cells are in excellent agreement with previous experiments in COS-1 cells (5). The main difference lies in the analysis technique employed in both studies. While the earlier study is based on PCH analysis, the current study uses Q_τ analysis. These experiments serve to demonstrate that Q_τ analysis is a viable technique for the study of protein interactions in living cells.

DISCUSSION

Mandel's Q-parameter uses the first two moments of the photon counts to specify the brightness of a sample. Here, we extend the definition of Mandel's Q-parameter by introducing Eq. 5. As a consequence, the Q-parameter is now a function of the lag time τ between photon counts. For $\tau = 0$ we recover the original definition of the Q-parameter, which we refer to as Q_0 to distinguish it from the case $\tau > 0$. The simple relationship of Eq. 2 between Q_0 and the brightness is only valid in the limit of short sampling times and in the absence of nonideal detector effects. These conditions are usually not fulfilled in actual experiments. We previously described a model that describes the influence of dead time and afterpulsing on the brightness and Q_0, but ignored sampling time effects. Here we extended the theory by taking undersampling, dead time, and afterpulsing into account. To describe the experimental data required the modeling of dead-time effects to second order in δ. We demonstrated that the theory successfully describes experimental data and recovers the brightness of the sample.

We also developed the theory of the generalized Q-parameter for $\tau > 0$ that takes undersampling, dead time, and afterpulsing into account. The generalized Q-parameter for $\tau > 0$ is denoted Q_τ. We noticed that Q_τ offers many advantages over Q_0 analysis. First, dead time causes much smaller changes in the value of Q_τ than in the value of Q_0. Consequently, first-order effects in δ are sufficient to describe dead-time-affected Q'_τ. Second, for brightnesses typically encountered in FFS experiments, the relative deviation of Q_τ introduced by dead time only depends on the fluorescence intensity, which allowed us to simplify the model significantly (see Eq. 42). Equation 42 only requires the calculation of the normalized correlation function $f_{\mathrm{T}}^{(\mathrm{r})}$ of second order, whereas Q_0 analysis requires the calculation of $f_{\mathrm{T}}^{(\mathrm{r})}$ up to the forth order. In contrast to Q_τ, the dead-time-induced relative deviation of Q_0 depends on brightness and increases with decreasing brightness. These facts illustrate that Q_τ analysis is significantly more robust than Q_0 analysis in the presence of dead time as illustrated in Fig. 7.

Third, in contrast to Q_0 analysis the effect of afterpulsing on Q_τ is very small and can be safely ignored. Our derivation of afterpulsing effects on Q_τ assumes sampling times that are larger than the timescale of afterpulse generation. For our detector all afterpulses follow within a few microseconds. Because our sampling times are 10 μs and longer, the assumption is fulfilled.

In principle Q_τ can be evaluated for any $\tau > 0$. Because our sampling time T is finite, only discrete times $\tau = nT$ with $n \in \mathbb{N}$ are accessible. We usually determine $Q_\tau(T)$, which corresponds to the shortest τ allowed ($n = 1$). There is no advantage in using longer times. In fact, the value of $Q_\tau(\tau)$ decays rapidly with increasing τ. In other words, the signal used to determine the brightness is strongest for $Q_\tau(T)$.

The generalization of Mandel's parameter uses the correlation between photon counts separated in time by τ and is therefore related to the second-order autocorrelation function $g_{\mathrm{I}}(\tau)$ of the fluorescence intensity. Because FCS theory is based on the intensity I and not the integrated intensity W, the FCS correlation function has to be determined in the short sampling time limit. Commercial acquisition systems typically sample with a time resolution of tens of nanoseconds and provide the user with correlation functions that are virtually free from undersampling effects. We, on the other hand, determine $Q_\tau(T)$ using much longer sampling times T, which typically range from tens of microseconds to milliseconds. Because of the undersampling effect on $Q_\tau(T)$ the relation to the autocorrelation function is given by

$$Q(\tau) = \frac{\langle I \rangle}{T} \int_{-\mathrm{T}}^{\mathrm{T}} (T - |t|) g_{\mathrm{I}}(\tau + t) dt. \qquad (46)$$

Thus, to obtain the generalized Q-parameter by FCS one needs to evaluate Eq. 46 with the experimental realization of $g_{\mathrm{I}}(\tau)$. Of course, the experimentally obtained $g_{\mathrm{I}}(\tau)$ is also affected by dead time and afterpulsing. Methods to correct for these nonideal effects are available (25–27). However, if one has access to a record of the detected counts, it is much more convenient to directly calculate $Q_\tau(T)$ from the photon counts, as we have done here.

Let us briefly discuss the short sampling time limit of $Q(\tau)$. Because no undersampling of the generalized Q-parameter

occurs, its relationship to the autocorrelation function simplifies to $Q(\tau) = \langle I \rangle T\, g_I(\tau)$. In this limit, $g_I(\tau)$ and $Q(\tau)$ are proportional to one another. In other words, there is no advantage of using $Q(\tau)$ over the autocorrelation function. Thus, the brightness of a fluorophore can be determined by fitting the autocorrelation function to a model to determine the fluctuation amplitude $g(0)$. Care has to be exercised in determining $g(0)$, because dead time and afterpulsing affect the correlation function. Because the fluctuation amplitude of a single species is directly proportional to the number of molecules in the observation volume, $g(0) = \gamma_2/N$, the brightness is determined by $\lambda = \langle I \rangle g(0)/\gamma_2$. This is the standard method of determining the brightness from the autocorrelation function (28).

However, we do not use the short sampling time limit, but evaluate $Q_\tau(T)$ for long sampling times for two reasons. First, as we discussed earlier we essentially get rid of afterpulsing effects by choosing sampling times >10 μs. In fact, undersampling provides a general and convenient way to effectively ''integrate out'' any fast process. If the characteristic timescale of fluctuations for a given physical process is τ_C, when choosing a sampling time $T \gg \tau_C$ leads to a small amplitude of the photon count correlation $\langle \Delta k(t) \Delta k(t+T) \rangle$, because the signal is essentially uncorrelated for a lag time of T. As a consequence the value of $Q_\tau(T)$ is nearly unaffected by a physical process if $T \gg \tau_C$. ''Integrating out'' fast process simplifies the analysis of $Q_\tau(T)$. Second, increasing the sampling time leads to significant improvements in the signal/noise ratio (SNR) of $Q_\tau(T)$. The number of photons detected from a single molecule per sampling time T is denoted as ε. This parameter is important because the SNR of correlation functions improves with increasing ε (27,29). Choosing longer sampling times increases the value of ε. In the short sampling time limit ε is proportional to T (Eq. 1). The relationship between ε and T for arbitrary sampling times is reported elsewhere (4,30). This improvement of the SNR is especially crucial for cellular applications, where low excitation power and the intrinsic properties of fluorescent proteins lead to much smaller brightness values than typically encountered for in vitro measurements. We found that analyzing intracellular brightness by evaluating $g(0)$ from a fit of the autocorrelation function is indeed considerably less robust than $Q_\tau(T)$ analysis. $Q_\tau(T)$ analysis on the other hand is sufficiently robust to allow the direct determination of the brightness according to Eqs. 5 and 42. No fit is performed, because $Q_\tau(T)$ is based on a single calculated value, and the sampling time can be chosen at will so as to optimize the signal/noise. The sampling time dependence of the SNR of the second photon count moment was recently discussed (31).

The Q-parameter has an advantage over brightness, because it is directly determined from experimental values. Thus, Mandel's Q-parameter is in contrast to the brightness λ model independent. By choosing a model for the PSF the Q-parameter is related to the brightness by the factor γ_2 according to Eq. 2. The Q-parameter is determined from the first two moments of the photon counts. We introduced undersampling to increase its SNR. In addition, we substituted the second-order moment of the photon counts by its correlation to significantly decrease the influence of nonideal detector effects on the value of the Q-parameter. Thus, $Q_\tau(T)$ analysis combines elements of moment and FCS analysis.

We use a 3DG PSF to describe the data. To model Q_τ requires according to Eq. 42 the second-order function $f_T^{(2)}(\tau)$. The evaluation of $f_T^{(2)}(\tau)$ for a 3DG PSF requires numerical integration of Eq. 27 after inserting the correlation function $f_{3DG}^{(2)}(\tau)$ (see Eq. 26). The squared beam waist ratio of our instrument is around 25. The correlation functions for a 3DG and a 2DG model ($f_{3DG}^{(2)}(\tau)$ and $f_{2DG}^{(2)}(\tau)$) are very similar at early times, but differ slightly in their tail. Thus the integrated function $f_{T,2DG}^{(2)}(\tau)$ for 2DG provides a good approximation for $f_{T,3DG}^{(2)}(\tau)$ as long as undersampling is not too severe and $\tau = T$. We confirmed numerically that for undersampling factors of less than four the 2DG model provides a good approximation. The advantage of using $f_{2DG,T}^{(2)}(\tau)$ is that numerical integration is not needed, because Eq. 28 provides an analytical expression. As mentioned earlier the diffusion time τ_D, which is required for the evaluation of $f_{2DG,T}^{(2)}(\tau)$, is determined by fitting the autocorrelation function of the data. It is best to also employ a 2DG correlation function for determining the diffusion time, to be consistent.

In the presence of multiple species Q_τ analysis uses the same equation valid for a single species and simply returns the apparent brightness of the mixture. There is a small bias term, which as we discussed is much smaller than the experimental error, and is safely ignored. We previously used PCH analysis to determine the brightness (3,32). Models that account for dead time and afterpulsing have been recently introduced as well (14). PCH has an advantage over Q_τ analysis, because it allows the resolution of the brightnesses of a mixture, whereas Q_τ analysis only returns the apparent brightness of the mixture without resolving its components. However, the direct resolution of species requires an excellent signal/noise ratio of the data. The statistics for FFS experiments in cells is relatively poor, because of the low brightness of fluorescent proteins and the high fluorophore concentrations encountered. Consequently, PCH fails to resolve mixtures directly and instead only returns the apparent brightness of the mixture (5). Thus, with respect to experiments in cells Q_τ analysis appears as powerful as PCH analysis. An advantage of Q_τ analysis is that it is relatively straightforward to implement, whereas PCH analysis in the presence of dead time and afterpulsing requires more sophisticated algorithms. In addition, no afterpulsing correction is required for Q_τ, whereas afterpulsing needs to be accounted for in PCH. Thus, Q_τ is a convenient and robust technique that replaces PCH for in vivo titration studies where the signal/noise ratio is too low for PCH to resolve species directly.

Finally, we applied Q_τ analysis to measure the brightness of EGFP in cells as a function of protein concentration and observed the change in brightness of RXRLBD in CV-1 cells, which indicates the presence of homodimerization of the receptor. These experiments, which are similar to earlier studies using the PCH technique, demonstrate that Q_τ analysis is suitable for the study of protein-protein interactions in cells.

SUMMARY

Mandel's Q-parameter uses photon count moments to determine the brightness of a fluorophore. We define a generalized form of the Q-parameter Q_τ that introduces photon count correlations and explicitly depends on the correlation time τ. For $\tau = 0$ we recover the original definition of Mandel's Q-parameter Q_0. We develop and experimentally verify models for Q_0 and Q_τ that take dead time, afterpulsing, and sampling time effects into account. There are a number of advantages of Q_τ over the traditional parameter Q_0. The effect of dead time on Q_τ is significantly less than on Q_0, which leads to a rather robust and simple dead-time analysis of Q_τ. The effect of afterpulsing on Q_τ can be safely ignored, whereas it has to be taken explicitly into account for Q_0 analysis. If a mixture of species is present, Q_τ determines the apparent brightness of the mixture and provides an alternative to PCH if the signal/noise ratio of the experiment is too low to resolve species by PCH. Such conditions are frequently encountered in cellular FFS experiments. Here, Q_τ analysis provides an attractive alternative to PCH analysis, because it is easy to implement, requires no afterpulsing correction, and is quite robust with respect to dead-time effects.

APPENDIX A

Relations between cumulants and raw moments are conveniently calculated using the software MathStatica (Mathstatica, Sydney, Australia),

$$\begin{aligned}\langle\langle W\rangle\rangle &= \langle W\rangle\\ \langle\langle W_0 W_\tau\rangle\rangle &= \langle W_0 W_\tau\rangle - \langle W\rangle^2\\ \langle\langle W_0^2 W_\tau\rangle\rangle &= \langle W_0^2 W_\tau\rangle - \langle W\rangle(2\langle W_0 W_\tau\rangle + \langle W\rangle^2) - \langle W\rangle^3. \quad (47)\end{aligned}$$

For a single molecule diffusing through a volume V, the expressions for the integrated intensity moments is given by:

$$\langle W_{t_1} W_{t_2} \ldots W_{t_r}\rangle^{(1)} = \int_{t_1}^{t_1+T} dt_1 \int_{t_2}^{t_2+T} dt_2 \ldots \int_{t_r}^{t_r+T} dt_r \langle I(t_1^*) I(t_2^*) \ldots I(t_r^*)\rangle_i = \gamma_r (\lambda T)^r \frac{V_{PSF}}{V} \int_{t_1}^{t_1+T} dt_1 \int_{t_2}^{t_2+T} dt_2 \ldots \times \int_{t_r}^{t_r+T} dt_r f^{(r)}(t_1, t_2, \ldots, t_r) = \gamma_r (\lambda T)^r \frac{V_{PSF}}{V} f_T^{(r)}(t_1, t_2, \ldots, t_r). \quad (48)$$

For a stationary process the autocorrelation function only depends on time differences. As a result, we write $f^{(r)}(t_1, t_2, \ldots, t_r) = f^{(r)}(\tau_2, \ldots, \tau_r)$, and $f_T^{(r)}(t_1, t_2, \ldots, t_r) = f_T^{(r)}(\tau_2, \ldots, \tau_r)$, with $\tau_i = t_i - t_{i-1}$. The integrated intensity cumulant for a single molecule is given by Muller (4)

$$\langle\langle W_{t_1} W_{t_2} \ldots W_{t_r}\rangle\rangle^{(1)} = \langle W_{t_1} W_{t_2} \ldots W_{t_r}\rangle^{(1)} + \sum_{m\geq 2} \frac{f_m}{V^m}, \quad (49)$$

where the exact form of the functions f_m is not of interest here. The cumulant for a sample with N_{total} molecules in volume V is

$$\begin{aligned}\langle\langle W_{t_1} W_{t_2} \ldots W_{t_r}\rangle\rangle &= N_{total}\langle\langle W_{t_1} W_{t_2} \ldots W_{t_r}\rangle\rangle^{(1)}\\ &\quad + N_{total} \sum_{m\geq 2} \frac{f_m}{V^m} = \gamma_r (\lambda T)^r c V_{PSF}\\ &\quad f_T^{(r)}(t_1, t_2, \ldots, t_r) + c \sum_{m\geq 2} \frac{f_m}{V^{m-1}}, \quad (50)\end{aligned}$$

where we introduced the concentration of the sample, $c = N_{total}/V$. In fluorescence fluctuation experiments we measure fluorescence emerging from an open excitation volume, which is much smaller than the total sample volume V. We express the assumption of a very large surrounding volume, by taking the limit $1/V \to 0$. Note, that the concentration of the sample, which is an intensive quantity, is unchanged. The integrated intensity cumulant is now given by

$$\langle\langle W_{t_1} W_{t_2} \ldots W_{t_r}\rangle\rangle = \gamma_r (\lambda T)^r c V_{PSF} f_T^{(r)}(t_1, t_2, \ldots, t_r). \quad (51)$$

It is customary in fluorescence fluctuation spectroscopy to express the concentration c in terms of the average number of molecules N in the PSF volume, $N = cV_{PSF}$. This allows us to write the integrated intensity cumulant in its final form (see Eq. 21).

APPENDIX B

We derive an expression for Q_0' to second order of δ using the same steps used to derive an expression for Q_τ'. Taylor expansion of $P'(k|W)$ to second order in δ yields

$$P'(k|W) \simeq Poi(k, W) \cdot \left(1 + \delta[kW - k(k-1)] + \frac{\delta^2}{2} \times [k^2W^2 - kW(2k^2 - 2k + 1) + k(k-1)^3]\right), \quad (52)$$

and the corresponding first two dead-time-affected moments in k are related to ideal moments of W by

$$\begin{aligned}\langle k\rangle' &= \langle W\rangle - \delta\langle W^2\rangle + \frac{1}{2}\delta^2(\langle W^2\rangle + 2\langle W^3\rangle)\\ \langle k^2\rangle' &= \langle W\rangle + \langle W^2\rangle - \delta(3\langle W^2\rangle + 2\langle W^3\rangle)\\ &\quad + \frac{1}{2}\delta^2(3\langle W^2\rangle + 14\langle W^3\rangle + 6\langle W^4\rangle). \quad (53)\end{aligned}$$

We convert the ordinary moments of W into integrated intensity cumulants, using the transformation:

$$\begin{aligned}\langle\langle W\rangle\rangle &= \langle W\rangle\\ \langle\langle W^2\rangle\rangle &= \langle \Delta W^2\rangle - \langle W\rangle\\ \langle\langle W^3\rangle\rangle &= \langle \Delta W^3\rangle - 3\langle \Delta W^2\rangle + 2\langle W\rangle\\ \langle\langle W^4\rangle\rangle &= \langle \Delta W^4\rangle - 6\langle \Delta W^3\rangle - 3\langle \Delta W^2\rangle^2 + 11\langle \Delta W^2\rangle - 6\langle W\rangle.\end{aligned} \tag{54}$$

Now, combining Eq. 54 with Eq. 51, we write the moments as:

$$\begin{aligned}\langle W\rangle &= \lambda TN\\ \langle W^2\rangle &= (\lambda T)^2(\gamma_2 N f_{\mathrm{T}}^{(2)}(0) + N^2)\\ \langle W^3\rangle &= (\lambda T)^3(\gamma_3 N f_{\mathrm{T}}^{(3)}(0,0) + 3\gamma_2 N^2 f_{\mathrm{T}}^{(2)}(0) + N^3)\\ \langle W^4\rangle &= (\lambda T)^4(\gamma_4 N f_{\mathrm{T}}^{(4)}(0,0,0) + 4\gamma_3 N^2 f_{\mathrm{T}}^{(3)}(0,0)\\ &\quad + 3[\gamma_2 N f_{\mathrm{T}}^{(2)}(0)]^2 + 6N^3\gamma_2 f_{\mathrm{T}}^{(2)}(0) + N^4).\end{aligned} \tag{55}$$

Finally, inserting Eqs. 53 and 54 into Eq. 10, we arrive at Eq. 25.

APPENDIX C

We make the following approximations: i), all of the afterpulses detected during one sampling time interval are caused by real photoelectron events of the same sampling period. This is true when the sampling time T is larger than the characteristic decay time of the afterpulse autocorrelation function; ii), every single real event can only trigger one afterpulse at most. The total number of events k_{t}^* detected during a sampling time interval is

$$k_{\mathrm{t}}^* = \xi_{\mathrm{t}} + k_{\mathrm{t}}, \tag{56}$$

where k_{t} denotes the number of real events and ξ_{t} denotes the afterpulses. The correlation $\langle k_0^* k_\tau^*\rangle$ is given by

$$\langle k_0^* k_\tau^*\rangle = \langle k_0 k_\tau\rangle + \langle \xi_0\xi_\tau\rangle + 2\langle k_0\xi_\tau\rangle, \tag{57}$$

where we used $\langle k_0\xi_\tau\rangle = \langle \xi_0 k_\tau\rangle$. The probability to detect ξ afterpulses during the sampling time T can be related to the integrated intensity probability distribution. First we note that

$$P(\xi|W) = \sum_{\mathrm{k}=\xi} P(\xi|k)\, Poi(k;W). \tag{58}$$

Under assumptions i and ii, the conditional probability to detect ξ afterpulses in the presence of k real events is Campbell (24)

$$P(\xi|k) = \frac{k!}{\xi!(k-\xi)!} P_{\mathrm{a}}^{\xi}(1-P_{\mathrm{a}})^{\mathrm{k}-\xi}, \tag{59}$$

where P_{a} is the probability that a photon event produces an afterpulse. Hence, we write

$$\begin{aligned}P(\xi) &= \int dW P(W) P(\xi|W)\\ &= \int dW \left[\sum_{\mathrm{k}=\xi} P(\xi|k) Poi(k;W)\right] P(W).\end{aligned} \tag{60}$$

We use this result to calculate the mean of the afterpulse distribution:

$$\langle \xi\rangle = \sum_{\xi=0}^{\infty} \xi P(\xi) = \int dW P(W) \sum_{\xi=0}^{\infty}\sum_{\mathrm{k}=\xi}^{\infty} \xi P(\xi|k) Poi(k;W). \tag{61}$$

Combining Eqs. 59 and 61, we find

$$\langle \xi\rangle = P_{\mathrm{a}}\langle W\rangle. \tag{62}$$

We extend the same procedure to bivariate moments, starting from the conditional probability to detect ξ_0 afterpulses in one sampling time period and ξ_τ in another sampling time period a time τ apart, given that the integrated intensity during the two sampling time periods are W_0 and W_τ

$$\begin{aligned}P(\xi_0|W_0;\xi_\tau|W_\tau) &= P(\xi_0|W_0)P(\xi_\tau|W_\tau)\\ &= \sum_{\mathrm{k}_0}^{\infty}\sum_{\mathrm{k}_\tau}^{\infty} P(\xi_0|k_0)P(\xi_\tau|k_\tau) Poi(k_0;W_0) Poi(k_\tau;W_\tau),\end{aligned} \tag{63}$$

where k_0 and k_τ are the number of photoelectrons detected in each sampling time period. The joint probability $P(\xi_0,\xi_\tau)$ is given by

$$P(\xi_0,\xi_\tau) = \iint dW_0 dW_\tau P(\xi_0|W_0;\xi_\tau|W_\tau). \tag{64}$$

Combining Eqs. 63 and 64 with Eq. 59, we find

$$\langle \xi_0\xi_\tau\rangle = \sum_{\xi_0}^{\infty}\sum_{\xi_\tau}^{\infty} \xi_0\xi_\tau P(\xi_0,\xi_\tau) = P_{\mathrm{a}}^2\langle W_0 W_\tau\rangle. \tag{65}$$

A similar strategy is used to express $\langle \xi_0 k_\tau\rangle$ as moments of the integrated intensity. We consider the probability of detecting ξ_0 afterpulses in one sampling period and k_τ photons in a sampling period a time τ apart,

$$\begin{aligned}P(\xi_0,k_\tau) &= \sum_{\mathrm{k}_0=\xi_0}^{\infty} P(k_0,k_\tau)P(\xi_0|k_0)\\ &= \iint dW_0 dW_\tau p(W_0,W_\tau)\left[\sum_{\mathrm{k}_0=\xi_0}^{\infty} Poi(k_0;W_0)\right.\\ &\quad \left.\times Poi(k_\tau,W_\tau)p(\xi_0|k_0)\right].\end{aligned} \tag{66}$$

By substituting Eq. 59 into Eq. 66 we find

$$\langle \xi_0 k_\tau\rangle = \sum_{\xi_0}^{\infty}\sum_{\xi_\tau}^{\infty} \xi_0 k_\tau P(\xi_0,k_\tau) = P_{\mathrm{a}}\langle W_0 W_\tau\rangle, \tag{67}$$

and as already discussed in Eq. 15, in absence of dead time

$$\langle k_0 k_\tau\rangle = \langle W_0 W_\tau\rangle. \tag{68}$$

Because $P_{\mathrm{a}} \ll 1$, we only keep terms of first order in P_{a}. Equation 57 becomes

$$\langle k_0^* k_\tau^*\rangle \simeq (1+2P_{\mathrm{a}})\langle W_0 W_\tau\rangle. \tag{69}$$

The afterpulse affected average $\langle k^*\rangle$ is determined from Eqs. 56 and 62

$$\langle k^*\rangle = (1+P_{\mathrm{a}})\langle W\rangle. \tag{70}$$

Hence, keeping only first-order terms in P_{a}, the afterpulse affected Q-function is finally written as

$$\begin{aligned}Q^*(\tau) &= \frac{\langle k_0^* k_\tau^*\rangle - \langle k_0^*\rangle^2}{\langle k_0^*\rangle} \approx \frac{\langle W_0 W_\tau\rangle - \langle W\rangle^2}{\langle W\rangle}(1+P_{\mathrm{a}})\\ &= Q(\tau)(1+P_{\mathrm{a}}).\end{aligned} \tag{71}$$

We also derive, following the same procedure as used above, the relative deviation introduced by afterpulsing on Q_0 for arbitrary sampling times,

$$\frac{\Delta Q_0^*}{Q_0} = \frac{Q_0^* - Q_0}{Q_0} = P_a\left(1 + \frac{2}{Q_0}\right) = P_a\left(1 + \frac{2}{\gamma_2 \lambda T f_T^{(2)}(0)}\right). \quad (72)$$

In the limit of short sampling times, $f_T^{(2)}(0) \approx 1$, and we recover the result found by Hillesheim and Mueller (14).

This work was supported by grants from the National Institutes of Health (GM64589) and the National Science Foundation (PHY-0346782). A.S.A. acknowledges support by a ''La Caixa'' Foundation Fellowship.

REFERENCES

1. Elson, E. L., and D. Madge. 1974. Fluorescence correlation spectroscopy. I. Conceptual basis and theory. *Biopolymers.* 12:1–27.
2. Magde, D., E. L. Elson, and W. W. Webb. 1974. Fluorescence correlation spectroscopy. II. An experimental realization. *Biopolymers.* 13:29–61.
3. Chen, Y., J. D. Müller, P. T. So, and E. Gratton. 1999. The photon counting histogram in fluorescence fluctuation spectroscopy. *Biophys. J.* 77:553–567.
4. Muller, J. D. 2004. Cumulant analysis in fluorescence fluctuation spectroscopy. *Biophys. J.* 86:3981–3992.
5. Chen, Y., L. N. Wei, and J. D. Muller. 2003. Probing protein oligomerization in living cells with fluorescence fluctuation spectroscopy. *Proc. Natl. Acad. Sci. USA.* 100:15492–15497.
6. Thompson, N. L., A. M. Lieto, and N. W. Allen. 2002. Recent advances in fluorescence correlation spectroscopy. *Curr. Opin. Struct. Biol.* 12:634–641.
7. Schwille, P. 2000. Cross-correlation analysis in FCS. *In* Fluorescence Correlation Spectroscopy, Theory and Applications. E. L. Elson and R. Rigler, editors. Springer, Berlin, Germany 360–378.
8. Thompson, N. L. 1991. Fluorescence correlation spectroscopy. *In* Topics in Fluorescence Spectroscopy. J. R. Lakowicz, editor. Plenum, New York, NY. 337–378.
9. Palmer III, A. G., and N. L. Thompson. 1989. Fluorescence correlation spectroscopy for detecting submicroscopic clusters of fluorescence molecules in membranes. *Chem. Phys. Lipids.* 50:253–270.
10. Berland, K. M., P. T. So, Y. Chen, W. W. Mantulin, and E. Gratton. 1996. Scanning two-photon fluctuation correlation spectroscopy: particle counting measurements for detection of molecular aggregation. *Biophys. J.* 71:410–420.
11. Palmer III, A. G., and N. L. Thompson. 1987. Molecular aggregation characterized by high order autocorrelation in fluorescence correlation spectroscopy. *Biophys. J.* 52:257–270.
12. Palmer III, A. G., and N. L. Thompson. 1989. High-order fluorescence fluctuation analysis of model protein clusters. *Proc. Natl. Acad. Sci. USA.* 86:6148–6152.
13. Bedard, G. 1967. Dead-time corrections to the statistical distributions of photoelectrons. *Proc. Phys. Soc.* 90:131–141.
14. Hillesheim, L. N., and J. D. Muller. 2003. The photon counting histogram in fluorescence fluctuation spectroscopy with non-ideal photodetectors. *Biophys. J.* 85:1948–1958.
15. Chen, Y., J. D. Müller, S. Y. Tetin, J. D. Tyner, and E. Gratton. 2000. Probing ligand protein binding equilibria with fluorescence fluctuation spectroscopy. *Biophys. J.* 79:1074–1084.
16. Qian, H. 1990. On the statistics of fluorescence correlation spectroscopy. *Biophys. Chem.* 38:49–57.
17. Qian, H., and E. L. Elson. 1990. On the analysis of high order moments of fluorescence fluctuations. *Biophys. J.* 57:375–380.
18. Mandel, L. 1979. Sub-Poissonian photon statistics in resonance fluorescence. *Opt. Lett.* 4:205–207.
19. Mandel, L. 1958. Fluctuations of photon beams and their correlations. *Proc. Phys. Soc.* 72:1037–1048.
20. O'Donnell, K. A. 1986. Correction of dead-time effects in photoelectric counting distributions. *J. Opt. Soc. Am.* 3:113–115.
21. Saleh, B. 1978. Photoelectron Statistics. Springer-Verlag, New York, NY.
22. Schatzel, K. 1990. Noise on photon correlation data. I. Autocorrelation functions. *Quantum Opt.* 2:287–305.
23. Kendall, M., A. Stuart, and J. K. Ord. 1987. Kendall's Advanced Theory of Statistics. Oxford University Press, New York, NY.
24. Campbell, L. 1992. Afterpulse measurement and corrections. *Rev. Sci. Instrum.* 65:5794–5798.
25. Zhao, M., L. Jin, B. Chen, Y. Ding, H. Ma, and D. Chen. 2003. Afterpulsing and its correction in fluorescence correlation spectroscopy experiments. *Appl. Opt.* 42:4031–4036.
26. Palmer 3rd, A. G., and N. L. Thompson. 1989. Intensity dependence of high-order autocorrelation functions in fluorescence correlation spectroscopy. *Rev. Sci. Instrum.* 60:624–633.
27. Koppel, D. E. 1974. Statistical accuracy in fluorescence correlation spectroscopy. *Phys. Rev. A.* 10:1938–1945.
28. Elson, E. L. 2001. Fluorescence correlation spectroscopy measures molecular transport in cells. *Traffic.* 2:789–796.
29. Saffarian, S., and E. L. Elson. 2003. Statistical analysis of fluorescence correlation spectroscopy: the standard deviation and bias. *Biophys. J.* 84:2030–2042.
30. Palo, K., U. Mets, S. Jager, P. Kask, and K. Gall. 2000. Fluorescence intensity multiple distributions analysis: concurrent determination of diffusion times and molecular brightness. *Biophys. J.* 79:2858–2866.
31. Wu, B., and J. D. Muller. 2005. Time-integrated fluorescence cumulant analysis in fluorescence fluctuation spectroscopy. *Biophys. J.* 89: 2721–35.
32. Chen, Y., J. D. Müller, Q. Ruan, and E. Gratton. 2002. Molecular brightness characterization of EGFP in vivo by fluorescence fluctuation spectroscopy. *Biophys. J.* 82:133–144.